KSS-10/-Hdg

NASA CR- 112315

THE USE OF LEVY-LEES VARIABLES IN THREE-DIMENSIONAL BOUNDARY-LAYER FLOWS

Final Report on Contract NAS1-11104
NASA Langley Research Center
Hampton, Virginia

(NASA-CR-112315) THE USE OF LEVY-LEES VARIABLES IN THREE-DIMENSIONAL BOUNDARY-LAYER FLOWS Final Report (Cincinnati Univ.) 73 p HC $5.75 CSCL 20D G3/12 N73-21277 Unclas 68617

Prepared by
Veer Narain Vatsa, Graduate Research Assistant
and
R.T. Davis, Professor and Head
Department of Aerospace Engineering
University of Cincinnati
Cincinnati, Ohio 45221

January 1973

ACKNOWLEDGEMENT

The authors wish to express thanks to Dr. Julius Harris of Langley Research Center for providing the inviscid data for the computations contained herein and also for his advice in many aspects of the computations.

ABSTRACT

A method for solving a general class of three-dimensional boundary layer flows is developed. In the development, Levy-Lees variables are extended to three-dimensions and equations are placed in these similarity variables. An implicit finite difference scheme which is stable for negative transverse velocities is used to solve these equations. The method developed is applied to obtain solutions for sharp and spherically blunted circular cones at angle of attack. Longitudinal and transverse distributions are presented for these cases. Good agreement is found with the results obtained by other numerical schemes and the experimental data of Tracy, for sharp circular cones at angle of attack. For spherically blunted cones at angle of attack, the results are in good agreement with axisymmetric sphere results up to the region where spherical symmetry holds.

TABLE OF CONTENTS

Chapter		Page
I	Introduction	1
II	Formulation of the Problem	4
III	Formulation of the Problem in Finite-Difference Form	17
IV	Solution Technique	29
V	Results and Discussion	36
	References	41
	Appendix A: Computer Code	A1

LIST OF FIGURES

Figure	Description	Page
2.1	Body Oriented Co-ordinate System	44
3.1	Finite Difference Scheme Used in General Case.	45
3.2a	Finite Difference Scheme Used When Similarity Exists in ξ-Direction.	46
3.2b	Finite Difference Scheme Used When Similarity Exists in η-Direction.	47
3.3	General Set Up for Step by Step Integration	48
4.1	Co-ordinate System Used for Specifying Inviscid Data for Symmetric Sphere and for General 3-D Body Geometry	49
4.2	Schematic Diagram Indicating the Three Regions Where Separate Polynomials are Used for Each Region to Obtain the Inviscid Pressure Data	50
5.1	Pressure Distribution on Sharp Circular Cone at 8° Angle of Attack.	51
5.2	Heat Transfer Rate Distribution on Sharp Circular Cone at 8° Angle of Attack	52
5.3	Longitudinal Skin Friction Distribution on Sharp Circular Cone at 8° Angle of Attack . .	53
5.4	Transverse Skin Friction Distribution on Sharp Circular Cone at 8° Angle of Attack . .	54

Figure	Description	Page
5.5	Schematic Diagram of Co-ordinates Used to Present Results for Spherically Blunted Cone at an Angle of Attack	55
5.6	Pressure Distribution for Blunted Cone at 8° Angle of Attack	56
5.7	Heat Transfer Rate Distribution for Blunted Cone at 8° Angle of Attack	57
5.8	Longitudinal Skin Friction Distribution for Blunted Cone at 8° Angle of Attack	58
5.9	Variation of Heat Transfer Rate, Longitudinal and Transverse Skin Friction Around Blunted Cone at 8° Angle of Attack	59
5.10	Pressure Distribution for Blunted Cone at 4° Angle of Attack	60
5.11	Heat Transfer Rate Distribution for Blunted Cone at 4° Angle of Attack	61
5.12	Longitudinal Skin Friction Distribution for Blunted Cone at 4° Angle of Attack	62
5.13	Variation of Heat Transfer Rate, Longitudinal and Transverse Skin Friction Around Blunted Cone at 4° Angle of Attack	63

NOMENCLATURE

$A_1 - A_{14}$	Coefficients used in (2.42) through (2.45) and defined by (2.46) through (2.59).
A_n, B_n, C_n, D_n	Coefficients in the difference equation (3.23) and defined by (3.24) through (3.27), (3.32) through (3.35), (3.40) through (3.43) or (3.49) through (3.52).
$A_{1n}, A_{2n}, A_{3n}, A_{4n}, A_{5n}$	Coefficients in the general form of the governing equation (3.04) and defined by (3.05) through (3.09), (3.10) through (3.14) and (3.15) through (3.19) for ξ-momentum, η-momentum and energy equation respectively.
C	Constant in Sutherland's viscosity law as stated in (2.62).
C^*	Constant in Sutherland's viscosity law as defined by (2.66).
C_p	Nondimensional specific heat at constant pressure.
C_{f_ξ}	Longitudinal skin friction coefficient defined by $\frac{1}{\sqrt{Re}} C_{f_\xi} = \frac{\tau_{w_\xi}}{\frac{1}{2}\bar{\rho}_\infty \bar{u}_\infty^2}$

C_{f_η}	Transverse skin friction coefficient defined by $$\frac{1}{\sqrt{Re}} C_{f_\eta} = \frac{\tau_{w_\eta}}{\frac{1}{2}\bar{\rho}_\infty \bar{u}_\infty^2}$$
E_n, F_n	Coefficients in the recursion relations (3.53) and defined by (3.56) and (3.57) respectively.
F	Nondimensional longitudinal velocity.
G	Nondimensional transverse velocity.
h_1, h_2, h_3	Nondimensional surface scale factors in $\bar{s}_1$, $\bar{s}_2$ and $\bar{s}_3$ directions respectively
$\bar{k}$	Thermal conductivity.
$\bar{L}$	Reference length.
ℓ	Nondimensional viscosity defined by (2.65).
ℓ'	Arc length.
M_∞	Free stream mach number.
Pr	Prandtl Number defined to be $$Pr = \frac{\bar{\mu}\,\bar{C}_p}{\bar{k}}$$
p	Nondimensional pressure.
q	A parameter defined by (2.37).
Q	Nondimensional heat transfer rate defined by $$\frac{1}{\sqrt{Re}} Q = \frac{\bar{Q}}{\bar{\rho}_\infty \bar{u}_\infty^3}$$

R	Gas constant.
Re	Reference Reynolds number.
$\bar{S}_1, \bar{S}_2, \bar{S}_3$	Arc lengths in ξ, η and ζ directions respectively.
t	Nondimensional temperature.
$\bar{t}_r$	Reference temperature defined by $\bar{t}_r = \frac{\bar{u}_\infty^2}{R}$
$\bar{u}_\infty$	Free stream velocity.
u	Nondimensional velocity component in ξ-direction.
v	Nondimensional velocity component in η-direction.
V	Transformed velocity in normal direction defined by (2.36).
w	Nondimensional velocity component in ζ-direction.
We	A velocity-like term and is a function of u_e.
Z	Transformed normal co-ordinate.
α	Angle of attack.
γ	Ratio of specific heats defined to be $\gamma = \frac{\bar{C}_p}{\bar{C}_v}$
λ	Crank-Nicolson Number.
ζ	Normal distance as shown in Fig. 2.1.

η	Surface co-ordinate as shown in Fig. 2.1.
θ	Nondimensional temperature defined by $\theta = t/t_e$.
μ	Nondimensional viscosity defined by (2.63).
$\overline{\mu}_r$	Reference viscosity evaluated at the temperature $\overline{t}_r$.
ξ	Surface co-ordinate as shown in Fig. 2.1.
$\overline{\rho}_\infty$	Free stream density.
ρ	Nondimensional density.
τ_{w_ξ}	Wall shear stress component in ξ-direction.
τ_{w_η}	Wall shear stress component in η-direction.
ϕ	Similarity parameter used for transformation of the normal co-ordinate (2.31) and defined by (2.41).
W	Variable used to represent F, G or θ in (3.04) to reduce the governing equations to a general form.
$\Delta\xi$	Step size in ξ-direction.
$\Delta\eta$	Step size in η-direction.
ΔZ	Step size in normal (Z) direction.

Subscripts

e	Inviscid condition at the body surface.
w	Conditions at the body surface

o	Stagnation conditions.
∞	Free stream conditions.

Superscripts

$\overline{}$	Dimensional quantity.

I. INTRODUCTION

The importance of three-dimensional effects in boundary layer theory has long been recognized, as indicated by the reviews of the literature by Cooke and Hall [1], Mager [2] and Stewartson [3]. Due to the complexities of these flows, the majority of the literature has been concerned with approximate methods or with treating limiting cases where the boundary layer equations reduce to quasi- two-dimensional form. Yen and Thyson [4] have used integral methods and have shown reasonable agreement with experimental heat transfer data. By far, the most popular method of solution has been developed through use of small cross flow theory, which reduces the equations to a quasi- two-dimensional form. Chan [5] has shown remarkable agreement of the small cross flow theory with experimental data.

As compared to two-dimensional boundary layers, relatively little work has been done on the computation of generalized three-dimensional boundary layers even for the simple case of the flow over axisymmetric bodies. Most of the work done in this area is restricted to only the windward plane of symmetry, e.g. Libby [6] and Watkins and Blottner [7]. Another case which has received considerable attention is that of the three-dimensional boundary layer on a conical body. The general approach here is to transform the governing equations so as to eliminate dependence on the streamwise independent variable as has been done by McGowan and Davis [8], Dwyer [9] and Boericke [10].

Der [11] has used an explicit method developed by Raetz [12] for solving the full three-dimensional boundary layer equations through use of zones of influence and dependence and the method has been applied to solve spherically blunted cone problems.

The approach used here will be very similar to that of McGowan and Davis [8] in as much as the finite difference scheme and the general solution technique is concerned. However, here we will use Levy Lees type variables rather than working with the Grocco type variables of ref. [8]. An implicit finite difference scheme suggested by Krause [13] will be used so that regions of negative transverse velocities can be handled with the stability problem practically eliminated.

The general three-dimensional boundary layer equations will first be specialized to Geodesic co-ordinates. A similarity type of transformation will then be introduced and the equations will be put in Levy Lees type of variables. Introduction of these variables will result in the correct similarity form of the equations, dependent only upon the normal transformed co-ordinate at stagnation points and sharp edges. Since the dependence on one co-ordinate drops out along the lines of symmetry, we can generate two planes of starting solutions originating at the sharp edge (or the stagnation point) from which the entire solution can be obtained using step-by-step integration.

The purpose of this investigation is to develop the three dimensional analogue of the Levy Lees variables that can be used for a general class of three-dimensional boundary layers and apply these to study the flow around sharp and spherically blunted circular cones at angle of attack. Calculations will first be made for 10° half-angle sharp circular cone at an angle of attack and the results will be compared with numerical calculations of McGowan and Davis [8]. The heat transfer data will be compared with experimental data of Tracy [14]. Flows around a spherically blunted cone of 10° half angle and at 4° and 8° angle of attack will be investigated and the results will be compared with the numerical results of Popinski [15]. The inviscid data for a sharp circular cone has been taken from numerical calculations of Jones [16] while for blunted cones the data has been taken from numerical calculations of Rakich and Cleary [17].

B

II. FORMULATION OF THE PROBLEM

The problem will now be put in a form suitable for finite-difference analysis. The governing equations will first be written in generalized body-oriented co-ordinates and then specialized to the Geodesic co-ordinate system. Finally, a Levy-Lees type of transformation will be introduced to put the equations in the similarity variables so that similar solutions can be obtained at proper points. As a result of this transformation, the boundary layer growth is practically eliminated.

The governing equations for three-dimensional compressible boundary layer flow in generalized body-oriented co-ordinates as shown in Figure 2.1, are given by Mager [2] as:

ξ-momentum

$$\frac{\bar{u}}{\bar{h}_1}\frac{\partial \bar{u}}{\partial \xi} + \frac{\bar{v}}{\bar{h}_2}\frac{\partial \bar{u}}{\partial \eta} + \frac{\bar{w}}{\bar{h}_3}\frac{\partial \bar{u}}{\partial \zeta} + \frac{\bar{u}\,\bar{v}}{\bar{h}_1\bar{h}_2}\frac{\partial \bar{h}_1}{\partial \eta} - \frac{\bar{v}^2}{\bar{h}_1\bar{h}_2}\frac{\partial \bar{h}_2}{\partial \xi}$$

$$= -\frac{1}{\bar{\rho}\bar{h}_1}\frac{\partial \bar{p}}{\partial \xi} + \frac{1}{\bar{\rho}\bar{h}_3}\frac{\partial}{\partial \zeta}\left[\frac{\bar{\mu}}{\bar{h}_3}\frac{\partial \bar{u}}{\partial \zeta}\right], \tag{2.01}$$

η-momentum

$$\frac{\bar{u}}{\bar{h}_1}\frac{\partial \bar{v}}{\partial \xi} + \frac{\bar{v}}{\bar{h}_2}\frac{\partial \bar{v}}{\partial \eta} + \frac{\bar{w}}{\bar{h}_3}\frac{\partial \bar{v}}{\partial \zeta} - \frac{\bar{u}^2}{\bar{h}_1\bar{h}_2}\frac{\partial \bar{h}_1}{\partial \eta} + \frac{\bar{u}\,\bar{v}}{\bar{h}_1\bar{h}_2}\frac{\partial \bar{h}_2}{\partial \xi}$$

$$= -\frac{1}{\bar{\rho}\bar{h}_2}\frac{\partial \bar{p}}{\partial \eta} + \frac{1}{\bar{\rho}\bar{h}_3}\frac{\partial}{\partial \zeta}\left[\frac{\bar{\mu}}{\bar{h}_3}\frac{\partial \bar{v}}{\partial \zeta}\right], \tag{2.02}$$

Energy

$$\frac{\bar{u}}{\bar{h}_1}\frac{\partial \bar{t}}{\partial \xi} + \frac{\bar{v}}{\bar{h}_2}\frac{\partial \bar{t}}{\partial \eta} + \frac{\bar{w}}{\bar{h}_3}\frac{\partial \bar{t}}{\partial \zeta}$$

$$= \frac{1}{\bar{C}_p\,\bar{\rho}}\left[\frac{\bar{u}}{\bar{h}_1}\frac{\partial \bar{p}}{\partial \xi} + \frac{\bar{v}}{\bar{h}_2}\frac{\partial \bar{p}}{\partial \eta}\right] + \frac{\bar{\mu}}{\bar{C}_p\bar{\rho}\bar{h}_3^{\,2}}\left[\left(\frac{\partial \bar{u}}{\partial \zeta}\right)^2 + \left(\frac{\partial \bar{v}}{\partial \zeta}\right)^2\right]$$

$$+ \frac{1}{\bar{C}_p\bar{\rho}\bar{h}_3}\frac{\partial}{\partial \zeta}\left[\frac{\bar{k}}{\bar{h}_3}\frac{\partial \bar{t}}{\partial \zeta}\right], \tag{2.03}$$

and Continuity

$$\frac{\partial}{\partial \xi}(\bar{h}_2\bar{h}_3\overline{\rho u}) + \frac{\partial}{\partial \eta}(\bar{h}_1\bar{h}_3\bar{V}) + \frac{\partial}{\partial \zeta}(\bar{h}_1\bar{h}_2\overline{\rho W}) = 0 \tag{2.04}$$

In addition, the equation of state and the viscosity law may be written as:

Equation of State

$$\bar{p} = \bar{\rho}\,\bar{R}\,\bar{T} \tag{2.05}$$

and Viscosity Law

$$\bar{\mu} = \bar{\mu}(\bar{T}) \tag{2.06}$$

Equations (2.01) through (2.06) are now nondimensionalized according to the following scheme:

$$h_1 = \frac{\bar{h}_1}{\bar{L}} , \tag{2.07}$$

$$h_2 = \frac{\bar{h}_2}{\bar{L}} , \tag{2.08}$$

$$h_3 = \frac{\bar{h}_3}{\bar{L}} \sqrt{Re} , \tag{2.09}$$

$$u = \frac{\bar{u}}{\bar{u}_\infty} , \tag{2.10}$$

$$v = \frac{\bar{v}}{\bar{u}_\infty} , \tag{2.11}$$

$$w = \frac{\bar{w}}{\bar{u}_\infty} \sqrt{Re} , \tag{2.12}$$

$$\mu = \frac{\bar{\mu}}{\bar{\mu}_r} , \tag{2.13}$$

$$\rho = \frac{\bar{\rho}}{\bar{\rho}_\infty} , \tag{2.14}$$

$$t = \frac{\bar{t}}{\bar{u}_\infty^2 / \bar{R}} , \tag{2.15}$$

$$p = \frac{\bar{p}}{\bar{\rho}_\infty \bar{u}_\infty{}^2} \quad , \tag{2.16}$$

and

$$C_p = \frac{\bar{C}_p}{\bar{R}} \quad , \tag{2.16a}$$

$$\text{where} \quad Re = \frac{\bar{\rho}_\infty \, \bar{u}_\infty \, \bar{L}}{\bar{\mu}_r} \tag{2.17}$$

In this scheme, Reynolds number is used in the nondimensionalization of h_3 and w purposely so that any explicit dependence of the final equations on the Reynolds number is eliminated.

Introducing equations (2.07) through (2.17) into the equations (2.01) through (2.06), we get the following set of nondimensional equations:

<u>ξ-momentum</u>

$$\frac{u}{h_1}\frac{\partial u}{\partial \xi} + \frac{v}{h_2}\frac{\partial u}{\partial \eta} + \frac{w}{h_3}\frac{\partial u}{\partial \zeta} - \frac{v^2}{h_1 h_2}\frac{\partial h_2}{\partial \xi} + \frac{uv}{h_1 h_2}\frac{\partial h_1}{\partial \eta}$$

$$= -\frac{1}{\rho h_1}\frac{\partial p}{\partial \xi} + \frac{1}{\rho h_3}\frac{\partial}{\partial \zeta}\left(\frac{\mu}{h_3}\frac{\partial u}{\partial \zeta}\right) \quad , \tag{2.18}$$

<u>η-momentum</u>

$$\frac{u}{h_1}\frac{\partial v}{\partial \xi} + \frac{v}{h_2}\frac{\partial v}{\partial \eta} + \frac{w}{h_3}\frac{\partial v}{\partial \zeta} - \frac{u^2}{h_1 h_2}\frac{\partial h_1}{\partial \eta} + \frac{uv}{h_1 h_2}\frac{\partial h_2}{\partial \xi}$$

$$= -\frac{1}{\rho h_2}\frac{\partial p}{\partial \eta} + \frac{1}{\rho h_3}\frac{\partial}{\partial \zeta}\left[\frac{\mu}{h_3}\frac{\partial v}{\partial \zeta}\right] \quad , \tag{2.19}$$

Energy

$$\frac{u}{h_1}\frac{\partial t}{\partial \xi} + \frac{v}{h_2}\frac{\partial t}{\partial \eta} + \frac{w}{h_3}\frac{\partial t}{\partial \zeta} = \frac{\gamma-1}{\gamma\rho}\left(\frac{u}{h_1}\frac{\partial p}{\partial \xi} + \frac{v}{h_2}\frac{\partial p}{\partial \eta}\right)$$

$$+ \frac{\gamma-1}{\gamma}\frac{\mu}{\rho h_3{}^2}\left[\left(\frac{\partial u}{\partial \zeta}\right)^2 + \left(\frac{\partial v}{\partial \zeta}\right)^2\right] + \frac{1}{\rho \Pr h_3}\frac{\partial}{\partial \zeta}\left(\frac{\mu}{h_3}\frac{\partial t}{\partial \zeta}\right) \quad , \tag{2.20}$$

Continuity

$$\frac{\partial}{\partial \xi}(h_2 h_3 \rho u) + \frac{\partial}{\partial \eta}(h_1 h_3 \rho v) + \frac{\partial}{\partial \zeta}(h_1 h_2 \rho w) = 0 \quad , \tag{2.21}$$

State

$$p = \rho t \quad , \tag{2.22}$$

and

Viscosity Law

$$\mu = \mu(t) . \tag{2.23}$$

In general, an infinitesimal arc length is given by

$$d\ell'^2 = (h_1 d\xi)^2 + (h_2 d\eta)^2 + (h_3 d\zeta)^2 \tag{2.24a}$$

If we take $d\xi$ to be the infinitesimal arc length along the surface in the streamwise direction, $h_1 = 1$ and assume the classical thin boundary layer approximation, $h_3 = 1$ equation (2.24a) may be written as

$$d\ell'^2 = (d\xi)^2 + h_2{}^2\,(d\eta)^2\,(d\zeta)^2 \tag{2.24b}$$

and we let

$$h_2 = h \tag{2.25}$$

Using (2.24) and (2.25), the governing equations (2.18) through (2.21) take the following form, whereas the equation of state and viscosity law are still represented by equations (2.22) and (2.23) respectively.

<u>ξ-momentum</u>

$$u \frac{\partial u}{\partial \xi} + \frac{v}{h} \frac{\partial u}{\partial \eta} + w \frac{\partial u}{\partial \zeta} - \frac{v^2}{h} \frac{\partial h}{\partial \xi}$$

$$= - \frac{1}{\rho} \frac{\partial p}{\partial \xi} + \frac{1}{\rho} \frac{\partial}{\partial \zeta} \left(\mu \frac{\partial u}{\partial \zeta}\right) \quad , \tag{2.26}$$

<u>η-momentum</u>

$$u \frac{\partial v}{\partial \xi} + \frac{v}{h} \frac{\partial v}{\partial \eta} + w \frac{\partial v}{\partial \zeta} + \frac{uv}{h} \frac{\partial h}{\partial \xi}$$

$$= - \frac{1}{\rho h} \frac{\partial p}{\partial \eta} + \frac{1}{\rho} \frac{\partial}{\partial \zeta} \left(\mu \frac{\partial v}{\partial \zeta}\right) \quad , \tag{2.27}$$

<u>Energy</u>

$$u \frac{\partial t}{\partial \xi} + \frac{v}{h} \frac{\partial t}{\partial \eta} + w \frac{\partial t}{\partial \zeta}$$

$$= \frac{(\gamma-1)}{\gamma\rho} \left(u \frac{\partial p}{\partial \xi} + \frac{v}{h} \frac{\partial p}{\partial \eta}\right) + \frac{(\gamma-1)}{\gamma} \frac{\mu}{\rho} \left[\left(\frac{\partial u}{\partial \zeta}\right)^2 + \left(\frac{\partial v}{\partial \zeta}\right)^2\right]$$

$$+ \frac{1}{\rho Pr} \frac{\partial}{\partial \zeta} \left(\mu \frac{\partial t}{\partial \zeta}\right) \quad , \tag{2.28}$$

and

Continuity

$$\frac{\partial}{\partial \xi}(h\rho u) + \frac{\partial}{\partial \eta}(\rho v) + \frac{\partial}{\partial \zeta}(h\rho w) = 0 \qquad (2.29)$$

or

$$h\rho w = -\frac{\partial}{\partial \xi}\int_o^{\zeta} h\rho u \, d\zeta - \frac{\partial}{\partial \eta}\int_o^{\zeta} \rho v \, d\zeta + h\rho_w W_w \qquad (2.30)$$

Introducing the following transformation in the normal direction

$$Z = \frac{W_e h}{\sqrt{2\phi}} \int_o^{\zeta} \rho \, d\zeta \qquad (2.31)$$

where

$$\phi = \phi(\xi,\eta) \quad \text{and} \quad W_e = W_e(u_e) \qquad (2.32)$$

and letting

$$F = \frac{u}{u_e}, \quad G = \frac{v}{v_e} \quad \text{and} \quad \theta = \frac{t}{t_e} \qquad (2.33a\text{-}c)$$

the continuity equation gives

$$h\rho w = -\frac{\partial}{\partial \xi}\left[\frac{u_e}{W_e}\sqrt{2\phi}\int_o^{Z} F dZ\right] - \frac{\partial}{\partial \eta}\left[\frac{v_e}{W_e}\frac{\sqrt{2\phi}}{h}\int_o^{Z} G dZ\right] + h\rho_w W_w$$

and since $\left(\frac{\partial}{\partial \xi}\right)_{\zeta,\eta} = \left(\frac{\partial}{\partial \xi}\right)_{\eta,Z} + \frac{\partial Z}{\partial \xi}\frac{\partial}{\partial Z}$ (2.34)

we get

$$h\rho w = -\frac{\partial}{\partial\xi}\left[\frac{u_e}{w_e}\sqrt{2\phi}\int_o^Z F dZ\right] - \frac{\partial Z}{\partial\xi}\frac{u_e}{w_e}\sqrt{2\phi}\,F$$

$$-\frac{\partial}{\partial\eta}\left[\frac{v_e}{w_e}\frac{\sqrt{2\phi}}{h}\int_o^Z G dZ\right] - \frac{\partial Z}{\partial\eta}\frac{v_e}{w_e}\frac{\sqrt{2\phi}}{h}G + h\,\rho_w W_w \tag{2.35}$$

Let us define a velocity-like term V as

$$V = -\frac{\sqrt{2\phi}}{q}\frac{\partial}{\partial\xi}\left[\frac{u_e}{w_e}\sqrt{2\phi}\int_o^Z F dZ\right] - \frac{\sqrt{2\phi}}{q}\frac{\partial}{\partial\eta}\left[\frac{v_e}{w_e}\frac{\sqrt{2\phi}}{h}\int_o^Z G dZ\right]$$

$$+ h\,\rho_w W_w \frac{\sqrt{2\phi}}{q} \tag{2.36}$$

where

$$q = \rho_e \mu_e W_e h^2 \tag{2.37}$$

Then the transformed continuity equation is

$$\frac{\partial V}{\partial Z} + \frac{\sqrt{2\phi}}{q}\left[\frac{\partial}{\partial\xi}\left(\frac{u_e}{w_e}\sqrt{2\phi}\,F\right) + \frac{\partial}{\partial\eta}\left(\frac{v_e}{w_e}\frac{\sqrt{2\phi}}{h}G\right)\right] = 0 \tag{2.38}$$

and the normal velocity component is given by

$$h\rho w = \frac{Vq}{\sqrt{2\phi}} - \frac{u_e}{w_e}\sqrt{2\phi}\frac{\partial Z}{\partial\xi}F - \frac{v_e}{w_e}\frac{\sqrt{2\phi}}{h}\frac{\partial Z}{\partial\eta}G \tag{2.39}$$

Using this transformed continuity equation, the convective operator takes the form

$$u\frac{\partial}{\partial\xi} + \frac{v}{h}\frac{\partial}{\partial\eta} + w\frac{\partial}{\partial\zeta} = u_e F\frac{\partial}{\partial\xi} + \frac{v_e G}{h}\frac{\partial}{\partial\eta} + \frac{w_e}{2\phi}Vq\frac{\partial}{\partial Z} \tag{2.40}$$

From similarity considerations, $\phi(\xi,\eta)$ is found to be of the form

$$\phi = \int_0^{\xi} \rho_e \mu_e W_e h^2 d\xi + q(\eta) \tag{2.41}$$

and W_e is chosen to be equal to u_e in our case.

Using the transformation of the normal co-ordinate (2.31) and the convective operator from (2.40) and letting

$$\ell = \frac{\rho\mu}{\rho_e \mu_e}$$

the governing equations take the form:

<u>ξ-momentum</u>

$$A_7 F \frac{\partial F}{\partial \xi} + A_1 (F^2 - \theta) + A_3 (FG - \theta) + A_4 G \frac{\partial F}{\partial \eta}$$

$$- A_5 (G^2 - \theta) + V \frac{\partial F}{\partial Z} = \frac{\partial}{\partial Z} (\ell \frac{\partial F}{\partial Z}) \tag{2.42}$$

<u>η-momentum</u>

$$A_7 F \frac{\partial G}{\partial \xi} + A_2 (G^2 - \theta) + (A_8 + A_{10})(FG - \theta)$$

$$+ A_4 G \frac{\partial G}{\partial \eta} + V \frac{\partial G}{\partial Z} = \frac{\partial}{\partial Z} (\ell \frac{\partial G}{\partial Z}) \tag{2.43}$$

<u>Energy Equation</u>

$$A_7 F \frac{\partial \theta}{\partial \xi} + A_{11} (F - G)\theta + A_4 G \frac{\partial \theta}{\partial \eta} + V \frac{\partial \theta}{\partial Z}$$

$$= \ell [A_{13} (\frac{\partial F}{\partial Z})^2 + A_{14} (\frac{\partial G}{\partial Z})^2] + \frac{1}{Pr} \frac{\partial}{\partial Z} (\ell \frac{\partial \theta}{\partial Z}) \tag{2.44}$$

and <u>Continuity Equation</u>

$$\frac{\partial V}{\partial Z} + \frac{\sqrt{2\phi}}{q}\left[\frac{\partial}{\partial \xi}(\sqrt{2\phi}\; F) + \frac{\partial}{\partial \eta}\left(\frac{v_e}{w_e}\frac{\sqrt{2\phi}}{h}\; G\right)\right] = 0 \tag{2.45}$$

The coefficients A_1-A_{14} depend only on the inviscid quantities and geometry and are defined as follows:

$$A_1 = \frac{2\phi}{qu_e}\frac{\partial u_e}{\partial \xi} \quad , \tag{2.46}$$

$$A_2 = \frac{2\phi}{qh}\frac{1}{u_e}\frac{\partial v_e}{\partial \eta} \quad , \tag{2.47}$$

$$A_3 = \frac{2\phi}{qh}\frac{v_e}{u_e^2}\frac{\partial u_e}{\partial \eta} \quad , \tag{2.48}$$

$$A_4 = \frac{2\phi}{qh}\frac{v_e}{u_e} \quad , \tag{2.49}$$

$$A_5 = \frac{2\phi}{qh}\frac{v_e^2}{u_e^2}\frac{\partial h}{\partial \xi} \quad , \tag{2.50}$$

$$A_6 = \frac{u_e}{w_e} = 1 \quad , \tag{2.51}$$

$$A_7 = \frac{2\phi}{q} \quad , \tag{2.52}$$

$$A_8 = \frac{2\phi}{q}\frac{1}{v_e}\frac{\partial v_e}{\partial \xi} \quad , \tag{2.53}$$

$$A_9 = h\,\frac{u_e}{v_e} \quad , \tag{2.54}$$

$$A_{10} = \frac{2\phi}{qh}\frac{\partial h}{\partial \xi} \quad , \tag{2.55}$$

$$A_{11} = -\frac{2\phi}{q}\frac{(\gamma-1)}{\gamma}\frac{1}{t_e}\left(u_e\frac{\partial u_e}{\partial \xi} + \frac{1}{\rho_e}\frac{\partial p_e}{\partial \xi} + v_e\frac{\partial v_e}{\partial \xi}\right) , \tag{2.56}$$

$$A_{12} = -A_{11} , \tag{2.57}$$

$$A_{13} = \frac{\gamma-1}{\gamma}\frac{u_e^2}{t_e} \tag{2.58}$$

and

$$A_{14} = \frac{\gamma-1}{\gamma}\frac{v_e^2}{t_e} . \tag{2.59}$$

For the starting point where $\xi = 0$, the values of these coefficients are determined by a limiting process.

The boundary conditions on F, G and θ are at $Z = 0$:

$$F = 0,$$

$$G = 0,$$

and

$$\theta = \frac{t_w}{t_e} \tag{2.60a-c}$$

where t_w is the wall temperature which is assumed specified and as $Z \to \infty$:

$$F = 1,$$

$$G = 1,$$

and

$$\theta = 1. \tag{2.61a-c}$$

The viscosity coefficient will be given by Sutherland's law:

$$\frac{\mu^*}{\mu_r} = \frac{(t_r+C)}{(t+C)} \left(\frac{t^*}{t_r}\right)^{3/2} \qquad (3.62)$$

where C is the Sutherland constant which is equal to 198.6°R for air.

Nondimensionalizing the temperature by $t_r = \frac{u_\infty^2}{R}$, we get

$$\mu = \left[\frac{1+C'}{t+C'}\right] t^{3/2} \qquad (2.63)$$

where $$C' = \frac{C}{u_\infty^2} R \qquad (2.64)$$

Therefore,

$$\ell = \frac{\rho\mu}{\rho_e\mu_e} = \left[\frac{1+C^*}{\theta+C^*}\right] \theta^{1/2} \qquad (2.65)$$

where $$C^* = \frac{C}{u_\infty^2} \frac{R}{t_e} . \qquad (2.66)$$

From (2.65), we get

$$\frac{1}{\ell}\frac{d\ell}{d\theta} = \frac{(C^*-\theta)}{2\theta(\theta+C^*)} . \qquad (2.67)$$

The nondimensional skin friction coefficients can be shown to be

$$C_{f_\xi} = 2\mu_e u_e \ell \frac{\partial F}{\partial Z} \frac{\rho_e\mu_e h}{\sqrt{2\phi}} , \qquad (2.68)$$

and

$$C_{f_\eta} = 2\mu_e \, v_{e\ell} \, \frac{\partial G}{\partial Z} \, \frac{\rho_e \mu_e \, h}{\sqrt{2\phi}} \, , \tag{2.69}$$

and the nondimensional heat transfer rate can be shown to be

$$Q = \frac{\gamma \, \mu_e}{(\gamma-1)Pr} \, t_{e\ell} \, \frac{\partial \theta}{\partial Z} \, \frac{\rho_e \mu_e \, h}{\sqrt{2\phi}} \quad . \tag{2.70}$$

Finally, the physical normal distance can be expressed as

$$\zeta = \int_o^Z \frac{\sqrt{2\phi}}{\rho_e u_e \, h} \, \Theta \, d \, Z \quad . \tag{2.71}$$

This formulation is very similar to that of McGowan and Davis [8] except for the fact that similarity variables are used here.

III. FORMULATION OF THE PROBLEM IN FINITE DIFFERENCE FORM

The numerical scheme used to solve the coupled nonlinear second-order partial differential equations (2.42) through (2.45) is presented here. In principle, these three equations are replaced by a set of consistent linearized algebraic equations. The linearization is achieved by updating the coefficients appearing in these equations through iteration. This set of equations is of tridiagonal form which can be solved easily for boundary conditions of the type (2.60) and (2.61).

The finite difference scheme used here is the one developed by Krause [13] and it can be used for negative transverse velocity regions. This being an implicit scheme, problems of stability and mesh size are greatly reduced. The set of finite difference equations so developed is uniformly valid to second-order in the mesh spacings of the finite difference grid. The general grid system used is shown in Fig. 3.1. The equations are written at the mid point (C,n) and solved for the quantities F, G and θ at the point $(2,n)$, assuming that these quantities are known from previous calculations at the points $(1,n)$, $(3,n)$ and $(4,n)$. After solving the energy, ξ-momentum and η-momentum equations, the continuity equation, which is a first-order partial differential equation, is solved at the mid point (C,n) subject to the boundary condition

$$\text{at } Z = 0 \qquad V(C,n) = 0.$$

An iterative scheme is used on all the 4 governing equations, until the value of skin friction differs very slightly from the previous calculations.

Three separate cases will be handled; a case in which similarity exists in both surface variables ξ and η, a case in which similarity exists in one of the surface variables, say ξ or η and a scheme to be used in general case. Before we discuss these cases, it will be more convenient to rearrange the equations (2.42) through (2.44) as follows:

ξ-momentum

$$\frac{\partial^2 F}{\partial Z^2} + \left[\frac{1}{\ell}\frac{d\ell}{d\theta}\frac{\partial \theta}{\partial Z} - \frac{V}{\ell}\right]\frac{\partial F}{\partial Z} - \left[\frac{A_1 F + A_3 G}{\ell}\right] F$$

$$+ (A_1\theta + A_3\theta - A_5\theta + A_5 G^2)\,\frac{1}{\ell} - \frac{A_7 F}{\ell}\frac{\partial F}{\partial \xi} - A_4\,\frac{G}{\ell}\frac{\partial F}{\partial \eta} = 0\ , \qquad (3.01)$$

η-momentum

$$\frac{\partial^2 G}{\partial Z^2} + \left[\frac{1}{\ell}\frac{d\ell}{d\theta}\frac{\partial \theta}{\partial Z} - \frac{V}{\ell}\right]\frac{\partial G}{\partial Z} - \frac{1}{\ell}\,(A_2 G + A_8 F + A_{10} F)\ G$$

$$+ (A_2 + A_8 + A_{10})\,\frac{\theta}{\ell} - \frac{A_7}{\ell}\,F\,\frac{\partial G}{\partial \xi} - \frac{A_4}{\ell}\,G\,\frac{\partial G}{\partial \eta} = 0 \qquad (3.02)$$

and

Energy Equation

$$\frac{\partial^2 \theta}{\partial Z^2} + \left[\frac{1}{\ell}\frac{d\ell}{d\theta}\frac{\partial \theta}{\partial Z} - Pr\,\frac{V}{\ell}\right]\frac{\partial \theta}{\partial Z} - A_{11}\,\frac{Pr}{\ell}\,(F-G)\,\theta$$

$$+ Pr\left[A_{13}\left(\frac{\partial F}{\partial Z}\right)^2 + A_{14}\left(\frac{\partial G}{\partial Z}\right)^2\right] - A_7\,\frac{Pr}{\ell}\,F\,\frac{\partial \theta}{\partial \xi} - A_4\,\frac{Pr}{\ell}\,G\,\frac{\partial \theta}{\partial \eta} = 0 \qquad (3.03)$$

Thus it is clear that if W represents F, G or θ, whichever is applicable, then all of these three equations can be written in the general form

$$\left.\frac{\partial^2 W}{\partial Z^2}\right|_n + A_{1n} \left.\frac{\partial W}{\partial Z}\right|_n + A_{2n} W_n + A_{3n}$$

$$+ A_{4n} \left.\frac{\partial W}{\partial \xi}\right|_n + A_{5n} \left.\frac{\partial W}{\partial \eta}\right|_n = 0 \tag{3.04}$$

where the coefficients A_{1n}, A_{2n}, A_{3n}, A_{4n} and A_{5n} are given by

For the <u>ξ-momentum</u> <u>equation</u>

$$A_{1n} = \frac{1}{\ell} \frac{d\ell}{d\theta} \frac{\partial \theta}{\partial Z} - \frac{V}{\ell} , \tag{3.05}$$

$$A_{2n} = - \frac{(A_1 F + A_3 G)}{\ell} , \tag{3.06}$$

$$A_{3n} = \frac{(A_1 \theta + A_3 \theta - A_5 \theta + A_5 G^2)}{\ell} , \tag{3.07}$$

$$A_{4n} = - \frac{A_7 F}{\ell} , \tag{3.08}$$

and

$$A_{5n} = - \frac{A_4 F}{\ell} , \tag{3.09}$$

For the <u>η-momentum</u> <u>equation</u>

$$A_{1n} = \frac{1}{\ell} \frac{d\ell}{d\theta} \frac{\partial \theta}{\partial Z} - \frac{V}{\ell} , \tag{3.10}$$

$$A_{2n} = - \frac{(A_2G+A_8F+A_{10}F)}{\ell} \quad , \tag{3.11}$$

$$A_{3n} = \frac{(A_2 + A_8 + A_{10})}{\ell} \, , \tag{3.12}$$

$$A_{4n} = - A_7 \frac{F}{\ell} \quad , \tag{3.13}$$

and

$$A_{5n} = - A_4 \frac{G}{\ell} \quad . \tag{3.14}$$

and for the <u>energy equation</u>

$$A_{1n} = \frac{1}{\ell} \frac{d\ell}{d\theta} \frac{\partial\theta}{\partial Z} - \frac{Pr}{\ell} V \quad , \tag{3.15}$$

$$A_{2n} = - \frac{Pr}{\ell} A_{11} \; (F-G) \quad , \tag{3.16}$$

$$A_{3n} = Pr \; [A_{13} \; (\frac{\partial F}{\partial Z})^2 + A_{14} \; (\frac{\partial G}{\partial Z})^2 \;] \quad , \tag{3.17}$$

$$A_{4n} = - Pr \; A_7 \frac{F}{\ell} \quad , \tag{3.18}$$

and

$$A_{5n} = - Pr \; A_4 \frac{G}{\ell} \quad . \tag{3.19}$$

The following discussion will refer to the general form (3.04) of the governing equations, rather than the original equations.

Case I. Solution at $\xi=0$ and $\eta=0$

This refers to the case where similarity exists in both the ξ and η directions. So the governing equations reduce to ordinary differential equations. In this case (1,n) coincides with (2,n) and (3,n) coincides with (4,n) because of the similarity in η-direction whereas (2,n) coincides with (3,n) because of similarity in ξ-direction. So the equations are written at the point (2,n) and the solutions are also generated at this point only. The non-zero partial derivatives in equation (3.04), which are now actually total derivatives, are of the form:

$$\left.\frac{\partial W}{\partial Z}\right|_{2,n} = \frac{W_{2,n+1} - W_{2,n-1}}{2\Delta Z} + 0(\Delta Z)^2 \quad , \tag{3.20}$$

and

$$\left.\frac{\partial^2 W}{\partial Z^2}\right|_{2,n} = \frac{W_{2,n+1} - 2W_{2,n} + W_{2,n-1}}{\Delta Z^2} + 0(\Delta Z)^2 \quad . \tag{3.21}$$

In this case, the governing equations are of the form

$$\left.\frac{\partial^2 W}{\partial Z^2}\right|_{n} + A_{1n} \left.\frac{\partial W}{\partial Z}\right|_{n} + A_{2n} W_n + A_{3n} = 0 \quad . \tag{3.22}$$

Substituting for $\frac{\partial^2 W}{\partial Z^2}$ and $\frac{\partial W}{\partial Z}$ from (3.20)-(3.21) into (3.22) we get the tridiagonal form.

$$A_n W_{2,n-1} + B_n W_{2,n} + C_n W_{2,n+1} = D_n \tag{3.23}$$

where

$$A_n = \left(\frac{1}{\Delta Z^2} - \frac{A_{1n}}{2\Delta Z}\right) \quad , \tag{3.24}$$

$$B_n = \left(- \frac{2}{\Delta Z^2} + A_{2n}\right) \quad , \tag{3.25}$$

$$C_n = \left(\frac{1}{\Delta Z^2} + \frac{A_{1n}}{2\Delta Z}\right) \quad , \tag{3.26}$$

and

$$D_n = - A_{3n} \quad . \tag{3.27}$$

Case II. Solution at $\xi=0$ or $\eta=0$

This refers to the case where similarity exists in either the ξ-direction or the η-direction. A Crank-Nicolson finite difference scheme is used for the case $\xi=0$, while a truely implicit-finite-difference scheme is used for $\eta=0$.

a. Similarity in the ξ-direction

In this scheme (Figure 3.2a), the equations are written at the point (C,n) and solved for the quantities F, G and θ at the point (2,n) knowing the solution at the point (1,n). The partial derivatives can be written in the form

$$W\Big|_{C,n} = \lambda W_{2,n} + (1-\lambda)\ W_{1,n} + 0(\Delta\eta)^2 \quad , \tag{3.28}$$

$$\frac{\partial W}{\partial Z}\Big|_{C,n} = \frac{\lambda(W_{2,n+1} - W_{2,n-1}) + (1-\lambda)(W_{1,n+1} - W_{1,n-1})}{2\Delta Z} + 0(\Delta\eta)^2 \ , \tag{3.29}$$

$$\left.\frac{\partial^2 W}{\partial Z^2}\right|_{C,n} = \frac{\lambda[W_{2,n+1}-2W_{2,n}+W_{2,n-1}] + (1-\lambda)[W_{1,n+1}-2W_{1,n}+W_{1,n-1}]}{\Delta Z^2}$$

$$+ 0(\Delta\eta)^2 \quad , \tag{3.30}$$

and

$$\left.\frac{\partial W}{\partial \eta}\right|_{C,n} = \frac{W_{2,n} - W_{1,n}}{\Delta\eta} + 0(\Delta\eta)^2 \tag{3.31}$$

where λ = Crank-Nicolson number.

Substituting these in the equation (3.04) and rearranging it in tridiagonal form, we get

$$A_n = \left(\frac{1}{\Delta Z^2} - \frac{A_{1n}}{2\Delta Z}\right)\lambda \quad , \tag{3.32}$$

$$B_n = \left(-\frac{2}{\Delta Z^2} + A_{2,n}\right)\lambda + \frac{A_{5,n}}{\Delta\eta} \; , \tag{3.33}$$

$$C_n = \left(\frac{1}{\Delta Z^2} + \frac{A_{1n}}{2\Delta Z}\right)\lambda \quad , \tag{3.34}$$

and

$$-D_n = A_{3,n} + (1-\lambda)\left(\frac{1}{\Delta Z^2} + \frac{A_{1n}}{2\Delta Z}\right) W_{1,n+1} + (1-\lambda)\left(-\frac{2}{\Delta Z^2} + A_{2n}\right)W_{1,n}$$

$$+ (1-\lambda)\left(\frac{1}{\Delta Z^2} - \frac{A_{1n}}{2\Delta Z}\right) W_{1,n-1} - \frac{A_{5n}}{\Delta\eta} W_{1,n} \tag{3.35}$$

b. <u>Similarity in η-direction</u>

Here the equations are written at the point (C,n) and solved for values at the point (2,n), knowing the solutions at the point (3,n). The finite-difference grid is shown in Figure 3.2b. The partial derivatives become

$$W\Big|_{C,n} = \frac{W_{2,n} + W_{3,n}}{2} + 0(\Delta\xi)^2 \quad , \tag{3.36}$$

$$\frac{\partial W}{\partial Z}\Big|_{C,n} = \frac{(W_{2,n+1} - W_{2,n-1} + W_{3,n+1} - W_{3,n-1})}{4\Delta Z} + 0(\Delta\xi)^2 \quad , \tag{3.37}$$

$$\frac{\partial^2 W}{\partial Z^2}\Big|_{C,n} = \frac{(W_{2,n+1} - 2W_{2,n} + W_{2,n-1} + W_{3,n+1} - 2W_{3,n} + W_{3,n-1})}{2\Delta Z^2}$$

$$+ 0(\Delta\xi)^2 \quad , \tag{3.38}$$

and

$$\frac{\partial W}{\partial \xi}\Big|_{C,n} = \frac{W_{2,n} - W_{3,n}}{\Delta\xi} + 0(\Delta\xi)^2 \quad . \tag{3.39}$$

Substituting these in the equation (3.04) and putting it in the tridiagonal form, we get

$$A_n = [\frac{1}{2\Delta Z^2} - \frac{A_{1n}}{4\Delta Z}] \quad , \tag{3.40}$$

$$B_n = [\frac{A_{2n}}{2} - \frac{1}{\Delta Z^2} + \frac{A_{4n}}{\Delta\xi}] \quad , \tag{3.41}$$

$$C_n = [\frac{1}{2\Delta Z^2} + \frac{A_{1n}}{4\Delta Z}] \quad , \tag{3.42}$$

and

$$-D_n = + A_{3,n} + W_{3,n+1}\left(\frac{1}{2\Delta Z^2} + \frac{A_{1n}}{4\Delta Z}\right) + W_{3,n}\left(-\frac{1}{\Delta Z^2} + \frac{A_{2n}}{2} - \frac{A_{4n}}{\Delta \xi}\right)$$

$$+ W_{3,n-1}\left(\frac{1}{2\Delta Z^2} - \frac{A_{1n}}{4\Delta Z}\right) \tag{3.43}$$

Case III. General Case, ξ70, η70

Here the equations are written at the point (C,n) and solved for the values at the point (2,n) knowing the solution at the points (1,n), (3,n) and (4,n). The finite difference scheme is sketched in Figure 3.1. The partial derivatives can be written as

$$W\Big|_{C,n} = \frac{W_{2,n} + W_{3,n}}{2} + 0(\Delta^2) \quad , \tag{3.44}$$

$$\frac{\partial W}{\partial Z}\Big|_{C,n} = \frac{\frac{\partial W}{\partial Z}\Big|_{2,n} + \frac{\partial W}{\partial Z}\Big|_{3,n}}{2} + 0(\Delta^2)$$

$$= \frac{W_{2,n+1} - W_{2,n-1} + W_{3,n+1} - W_{3,n-1}}{4\Delta Z} + 0(\Delta^2) \quad , \tag{3.45}$$

$$\frac{\partial^2 W}{\partial Z^2}\Big|_{C,n} = \frac{\frac{\partial^2 W}{\partial Z^2}\Big|_{2,n} + \frac{\partial^2 W}{\partial Z^2}\Big|_{3,n}}{2} + 0(\Delta^2)$$

$$= \frac{W_{2,n+1} - 2W_{2,n} + W_{2,n-1} + W_{3,n+1} - 2W_{3,n} + W_{3,n-1}}{2\Delta Z^2} + 0(\Delta^2) \quad , \tag{3.46}$$

$$\frac{\partial W}{\partial \xi}\Big|_{C,n} = \frac{W_{2,n} - W_{3,n}}{\Delta \xi} + 0(\Delta^2) \quad , \tag{3.47}$$

and

$$\left.\frac{\partial W}{\partial \eta}\right|_{C,n} = \frac{(W_{2,n}-W_{1,n}) + (W_{4,n}-W_{3,n})}{2\Delta\eta} + O(\Delta^2) \quad . \tag{3.48}$$

Substituting these into the governing equations and rearranging in the tridiagonal form, we get

$$A_n = [\frac{1}{2\Delta Z^2} - \frac{A_{1n}}{4\Delta Z}] \quad , \tag{3.49}$$

$$B_n = [\frac{A_{2n}}{2} - \frac{1}{\Delta Z^2} + \frac{A_{4n}}{\Delta\xi} + \frac{A_{5n}}{2\Delta\eta}] \quad , \tag{3.50}$$

$$C_n = [\frac{1}{2\Delta Z^2} + \frac{A_{1n}}{4\Delta Z}] \quad , \tag{3.51}$$

and

$$D_n = A_{3n} + (\frac{1}{2\Delta Z^2} + \frac{A_{1n}}{4\Delta Z})W_{3,n+1} + (\frac{1}{2\Delta Z^2} - \frac{A_{1n}}{4\Delta Z})W_{3,n-1}$$

$$- \frac{A_{5n}}{2\Delta\eta}W_{1,n} + (\frac{A_{2n}}{2} - \frac{1}{\Delta Z^2} - \frac{A_{4n}}{\Delta\xi} - \frac{A_{5n}}{2\Delta\eta})\ W_{3,n} \quad . \tag{3.52}$$

The solution of the equations of the tridiagonal form (3.23) can be obtained by the standard methods for solving a linear tridiagonal algebraic set of equations. Knowing the values of the dependent variables F, G and θ at $n=1$ and at $n=IE$ (corresponding to the wall and the outer edge of the boundary layer respectively) from the boundary conditions (2.60)-(2.61), each of the sets of equations represented by the general form (3.23) can be solved for IE-2, evenly spaced points from $n=2$, one step away from the wall, to the point $n=IE-1$, one step away from the outer edge of the boundary layer by applying

$$W_{2,n} = E_n W_{2,n+1} + F_n \tag{3.53}$$

which is the general solution of (3.23) as justified by Richtmeyer [18].

Making use of the boundary conditions (2.60)-(2.61) and the fact that (3.53) should hold independent of the step size, we get

$$E1 = 0 \tag{3.54}$$

for F, G and θ and

$$F1 = 0,\ 0,\ t_w \tag{3.55}$$

for F, G and θ respectively.

It can be shown that the following recursion relations hold

$$E_n = \frac{-C_n}{A_n E_{n-1} + B_n} \tag{3.56}$$

$$F_n = \frac{D_n - A_n F_{n-1}}{A_n E_{n-1} + B_n} \tag{3.57}$$

Thus, E_n and F_n can be calculated knowing E1 and F1 in addition to the coefficients A_n, B_n, C_n and D_n, and using the above recursion relations. Making use of the outer edge boundary condition, $W_{2,n}$ can be calculated at all the inner points of the mesh from the equation (3.53).

After solving the equations (3.04) in this manner, the coefficients $A_{1_n}, A_{2_n}, A_{3_n}, A_{4_n}$, and A_{5_n} appearing in the governing equations are recomputed, updating the variables wherever needed and the equations are solved again. This process is repeated until the desired accuracy is achieved.

General Solution Technique

The solution technique used here is similar to the one used by McGowan and Davis [8], i.e. a step-by-step integration is performed. As shown in Figure 3.3, two planes of starting solution are needed for such an integration scheme, along with the boundary conditions at the wall and at the outer edge of the boundary layer.

At the intersection of these starting planes, the solution must be independent of both ξ and η-co-ordinates. In the case of sharp cone, this occurs at the sharp point while for blunt body it occurs at the stagnation point. The solution technique for this case has been described under Case I in this chapter. Once the corner solution is obtained, the starting solution can be generated in η-plane at $\xi=0$, using the method discussed earlier in this chapter under Case II. Also, the starting solution is generated on a line of symmetry with respect to the ξ-axis or along the windward streamline in our case.

With the solutions known in these two starting planes, we proceed along constant ξ lines around the body (in the η-direction) and step down along the body (in the ξ-direction), once the solution in a particular ξ-plane is completed.

IV. SOLUTION TECHNIQUE

In this chapter we will discuss the treatment of the inviscid data and the details of the solution technique employed herein.

A. Inviscid Data

The inviscid data is treated in much the same manner as by McGowan and Davis [8]. Thus we take the pressure distribution from independent numerical solutions to the inviscid equations and then solve for the velocity distribution, such that it satisfies the Bernoulli Equation, longitudinal and transverse momentum equations and the isentropic relation, applied at the surface.

The compressible Bernoulli Equation applied at the surface is,

$$h_o = \frac{P_e}{\rho_e}\left(\frac{\gamma}{\gamma-1}\right) + \frac{u_e^2}{2} + \frac{v_e^2}{2} \tag{4.01}$$

The ξ-momentum equation applied at the surface is,

$$u_e \frac{\partial u_e}{\partial \xi} + \frac{v_e}{h}\frac{\partial u_e}{\partial \eta} - \frac{v_e^2}{h}\frac{\partial h}{\partial \xi} = -\frac{1}{\rho_e h}\frac{\partial P_e}{\partial \xi} \tag{4.02}$$

The η-momentum equation applied at the surface is,

$$u_e \frac{\partial u_e}{\partial \xi} + \frac{v_e}{h}\frac{\partial v_e}{\partial \eta} + \frac{u_e v_e}{h}\frac{\partial h}{\partial \xi} = -\frac{1}{\rho_e h}\frac{\partial P_e}{\partial \eta} \tag{4.03}$$

and the isentropic relation, assuming that the entropy is constant is,

$$k = \frac{P_e}{\rho_e{}^{\gamma}} \tag{4.04}$$

Differentiating (4.01) with respect to ξ

$$0 = \frac{\gamma}{\gamma-1} \quad \frac{\gamma-1}{\gamma} k^{\frac{1}{\gamma}} P_e^{-\frac{1}{\gamma}} \frac{\partial P_e}{\partial \xi} + u_e \frac{\partial u_e}{\partial \xi} + v_e \frac{\partial v_e}{\partial \xi}$$

and using (4.04), we get

$$- \frac{1}{\rho_e} \frac{\partial P_e}{\partial \xi} = u_e \frac{\partial u_e}{\partial \xi} + v_e \frac{\partial v_e}{\partial \xi} \quad . \tag{4.05}$$

Combining (4.05) with the ξ-momentum equation and rearranging

$$\frac{\partial u_e}{\partial \eta} - \frac{\partial}{\partial \xi} (h\ v_e) = 0 \tag{4.06}$$

which is the zero-vorticity equation applied at the surface.

Note that if we differentiate the Bernoulli Equation with respect to η and combine with the η-momentum equation we will obtain (4.06) again. Thus, if we solve the Bernoulli Equation, isentropic relation and zero-vorticity equation, the solution will automatically satisfy the ξ-momentum and η-momentum equations.

For the special case of a sharp cone, equation (4.06) reduces to the simple form

$$v_e = \frac{\partial u_e}{\partial \eta} \qquad (4.07)$$

because for this case

$$h = \xi$$

and $\frac{\partial v_e}{\partial \xi} = 0$ since there is no variation in stream properties along rays, for conical flow.

The general technique of generating the inviscid data from a specified pressure distribution has been described in detail by McGowan and Davis [8]. The same procedure is followed here for the sharp circular cone at an angle of attack and the pressure distribution for this case is taken from numerical calculations of Jones [16].

A slightly different approach is used for the case of a spherically blunted cone due to the nature of the problem. The pressure data for this case is taken from the numerical calculations of Rakich [17]. Up to the point where spherical symmetry exists, the data is specified in wind co-ordinates centered at the stagnation point (Figure 4.1) and from there onwards, the body-oriented co-ordinates, centered at the frontal point on the sphere are used for specifying the data. The data is specified in 7 planes evenly spaced around the body.

For the symmetric sphere, the data is fitted with least-squares method to an even 14th order polynomial of the form

$$P = P_o \; (1 - P_2 S^2 - P_4 S^4 \dots - P_{14} S^{14}) \qquad (4.08)$$

where S is measured from the stagnation point.

In order to perform the 3-D calculations in body-oriented co-ordinates, it is necessary to find an expression for the pressure distribution as a function of S' measured from the frontal point 0' as the origin.

An 11th order polynomial of the form

$$P = P_1 + P_2 S' + P_3 S'^2 + \ldots\ldots + P_{11} S'^{10} \qquad (4.09)$$

is found for each of the seven planes in which the pressure data is available. For increased accuracy, separate polynomials are found for the three regions marked I, II and III in Figure 4.2, along the body. The pressure derivative in the longitudinal direction $\frac{\partial P_e}{\partial \xi}$, is found by differentiating the expressions (4.08) or (4.09) analytically, in their respective regions.

Knowing the pressure distribution (P_e and $\frac{\partial P_e}{\partial \xi}$), the procedure for generating the inviscid data is the same as for the sharp circular cone, except for the fact that we use a more general equation (4.06), rather than the equation (4.07) (which is applicable only for conical flows), in addition to the Bernoulli Equation and the Isentropic relation.

Once the inviscid quantities are calculated at a convenient number of points around the body, a five-point Lagrangian interpolation is used to find the desired quantity, if the point of interest lies between the planes where inviscid data has been generated.

B. Solution to the Problem

As described under the section "General Solution Technique", the planes of starting solutions can be generated, making use of the fact that a similar solution exists at the windward streamline and then step-by-step integration can be performed making use of the boundary conditions at the wall and at the outer edge of the boundary layer. For the sharp cone, this procedure does not present any difficulties, but for blunted cones, some special attention is required to apply the technique.

As mentioned earlier, the starting solution is obtained at the stagnation point in the wind co-ordinate system (Figure 4.1). The symmetric sphere calculations are carried out up to $S=2\alpha$, in a two-dimensional manner. The quantities F, G and θ obtained from symmetric sphere calculations are stored as double arrays so that we can find their values as a function of the co-ordinates ξ and Z.

Once we reach $S=2\alpha$, we switch over to the body-co-ordinates. The starting solution in the plane $X' = 1 - \cos\alpha$, of constant ξ around the body in this new co-ordinate system is then determined by interpolating the results of the symmetric sphere calculations. Note that in this new co-ordinate system we have,

$$F' = F \;, \tag{4.10a}$$

$$G' = F \;, \tag{4.10b}$$

and

$$\theta' = \theta, \tag{4.10c}$$

where ' refers to the quantities in the new co-ordinates.

Once the starting solution in the plane $\xi =$ constant is known, the general technique of step-by-step integration, described earlier is used to march along the body.

A mention must be made of the manner in which the similarity parameter ϕ is handled in the new co-ordinates. The parameter ϕ is found to be of the form

$$\phi = \int_{o}^{\xi} \rho_e \mu_e u_e \, h^2 \, d\xi \ . \tag{4.11}$$

Let the calculation in a particular co-ordinate system be performed up to $\xi = \xi_o$. Then the expression (4.11) can be used to calculate ϕ up to the point where $\xi = \xi_o$.

Once we switch to a new co-ordinate system, the value of ϕ should be calculated using the expression

$$\phi = \phi_c + \int_{\xi_o}^{\xi} \rho_e \mu_e \, u_e \, h^2 \, d\xi \tag{4.12}$$

where ϕ_o is the value of ϕ in the starting plane $\xi = \xi_o$, obtained by using the equation (4.11), in the earlier co-ordinate system and integrating up to the point of interest in the starting plane. Knowing ϕ_o, the values of ϕ can be obtained in the new co-ordinates by direct application of the equation (4.12).

The value of h is determined using the expression for the arc length

$$d\ell'^2 = (d\xi)^2 + h^2(d\eta)^2 + dZ^2 \tag{4.13}$$

and it is found that

$h = \xi$ for sharp cone

while h = local radius for the blunted cone.

V. RESULTS AND DISCUSSION

We shall now discuss the results obtained for the particular cases solved. Comparison of heat transfer rates with experimental data will be made for sharp circular cones. The cases of sharp and blunted cones will be discussed separately.

A. Sharp Circular Cone at Angle of Attack

The case chosen here is one for which experimental data on heat transfer rate is available. The flow parameters for the case chosen are:

$M_\infty = 8.0,$

$\bar{t}_\infty = 84.2°R,$

$\bar{t}_w/\bar{t}_o = 0.46,$

$R = 1718\ ft^2/sec^2\text{-}°R,$

$Pr = 0.738,$

$C = 198.6°R,$

$\theta_C = 10°,$

$\alpha = 8°,$

and

$\gamma = 1.4.$

This particular case has been studied by Tracy [14]. The calculations are performed using 101 points evenly spaced in the normal direction and 31 points in the transverse direction, evenly spaced from $\eta=0$ to $\eta=\eta_{max}$.

The inviscid pressure data of Jones [16] was used for these calculations. In Fig. 5.1 is shown the comparison of the pressure distribution used with Tracy's experimental data [14] for $M_\infty = 7.95$. Heat transfer rate distribution, nondimensionalized by $q_o = -0.0550\sqrt{Re\xi}$ (which is the heat transfer rate for the circular cone at zero degree angle of attack) is shown in Figure 5.2. For comparison, numerical results of McGowan and Davis [8] and experimental results of Tracy [14] are plotted in the same figure. It is apparent that the results obtained are very close to the numerical results of McGowan and Davis [8], whereas agreement with experimental data is not as good, expecially near the windward and leeward regions. This could be due to differences in the pressure data of Jones [16] and Tracy [14].

In Figure 5.3, the longitudinal skin friction coefficient nondimensionalized by $C_{f_{\xi o}} = .40040$ (where $C_{f_{\xi o}}$ is the longitudinal skin friction coefficient for the circular cone at zero degree angle of attack) is shown. Numerical results of reference [8] are shown for comparison. The results obtained here are in good agreement for most of the region.

Figure 5.4 represents the transverse skin friction coefficient nondimensionalized by $C_{f_{\xi o}}$. Here also, the numerical results of reference [8] are presented for comparison and they show a close agreement with the results obtained here. In conclusion we can say that for the sharp circular cone used here, we are in good agreement with the numerical results of reference [8] and experimental results of reference [14].

B. Blunted Cone at Angle of Attack

The test quantities used for this case are:

$M_\infty = 8.0,$

$\bar{t}_\infty = 418.87°R,$

$\bar{t}_w/\bar{t}_o = 0.6,$

$R = 1718\ ft^2/sec^2{=}°R,$

$Pr = 0.7,$

$C = 198.6°R,$

$\theta_C = 10°,$

$\alpha = 8°$ and $4°$,

and

$\gamma = 1.4.$

The inviscid pressure distribution is taken from the computer calculations supplied by Rakich [17]. This pressure distribution, nondimensionalized by $\gamma P_\infty M_\infty^2$, is presented in Figures 5.6 (for $\alpha=8°$) and 5.10 (for $\alpha=4°$) for the windward and leeward planes. This inviscid pressure data, which is available for seven planes evenly distributed in the transverse direction from $\eta=0$ to $\eta=\eta_{max}$ is represented by polynomial expressions for each plane and the pressure for intermediate values of transverse co-ordinate η are obtained by five point Lagrangian Interpolation.

Figure 5.7 shows the heat transfer rate distribution along the body for the windward and leeward planes, for 8° angle of attack. Numerical results of Popinski [15] are also shown for comparison. Figure 5.8 shows the longitudinal skin friction distribution for the same case and again the numerical results of Popinski [15] are shown. It is found that there is a good qualitative similarity between the two sets of results but numerical values are off by a few percentage points. This can be attributed to the manner in which the pressure data is treated in the two methods. It is noted that there is a slight kink in the pressure data near the sonic line from where onwards a different method of generating the data is employed. The kink results in a discontinuity in the pressure derivative $\partial P_e/\partial \xi$ and it has been found necessary to smooth the pressure distribution in order to avoid fluctuations in skin friction in this region. The final results will therefore depend on the degree of smoothing employed for the pressure distribution.

Figure 5.9 shows the variation of heat transfer rate and the longitudinal and transverse skin friction distribution in the meridian direction for a station at S = 62° from the nose of the sphere.

The results for a blunted cone at 4° angle of attack are presented in Figures 5.11 (heat transfer rate distribution), 5.12 (longitudinal skin friction distribution) and 5.13 (variation of heat transfer rate and longitudinal and transverse skin friction distribution in meridian planes). Essentially, the same nature is exhibited by heat transfer rate and skin friction distribution as in the case of 8° angle of attack. But as expected, the difference in the values of heat transfer rate (or longitudinal skin friction) at the same longitudinal station for windward and leeward planes, in this case is smaller than in the case of 8° angle of attack.

REFERENCES

1. Cooke, J.C. and Hall, M.G., 1962. "Boundary Layers in Three Dimensions". Progress in Aeronautical Sciences: Boundary Layer Problems, edited by D. Kuchemann and A. Ferri, Vol. II, Pergamon Press, New York.
2. Mager, A., 1964, "Three-Dimensional Laminar Boundary Layers," High-speed Aerodynamics and Jet Propulsion: Theory of Laminar Flows, edited by F.K. Moore, Vol. IV, Princeton University Press, Princeton, New Jersey.
3. Stewartson, K., 1964. The Theory of Laminar Boundary Layers in Compressible Fluids, Oxford University Press.
4. Yen, S. and Thyson, N.A., 1963. "An Integral Method for Calculation of Supersonic Laminar Boundary Layer with Heat Transfer on Yawed Cone," AIAA Journal, Vol. 1, No. 3. pp. 672-675.
5. Chan, Y.Y. 1969. "An Experimental Study of a Yawed Circular Cone in Hypersonic Flows," AIAA Journal, Vol. 7, No. 10, pp. 2035-2037.
6. Libby, P.A. 1969. "Three-Dimensional Boundary Layer with Uniform Mass Transfer," The Physics of Fluids, 12: 408-417.
7. Watkins, C.B. and Blottner, F.G., 1972. "Three-Dimensional Effects of Electron Density in a Blunt Body Laminar Boundary Layer." To be published as "Sandia Laboratories, Technical Report .

8. McGowan III, J.J. and Davis, R.T., 1970. "Development of a Numerical Method to Solve the Three-Dimensional Compressible Laminar Boundary Layer Equations with Application to Elliptic Cones at Angle of Attack," A.R.L. 70-0341, Virginia Polytechnic Institute, Blacksburg, Virginia.

9. Dwyer, H.A., 1969. "The Analysis and Calculations of the Three-Dimensional Boundary Layer Over a Sharp Cone at Angle of Attack," Final Report Sandia Corporation Contract (48-7084).

10. Boericke, R.R. 1971. "Laminar Boundary Layer on a Cone at Incidence in Supersonic Flow," AIAA Journal, Vol. 9, No. 3, pp. 462-468.

11. Der, Joe, Jr. 1969. "A Study of General Three-Dimensional Boundary Layer Problems by an Exact Method," AIAA Paper No. 69-138.

12. Raetz, G.S., 1957. "A Method of Calculating Three-Dimensional Laminar Boundary Layers of Steady Compressible Flow," Report No. HAI-58-73 (BLC-114), Northrup Corporation.

13. Krause, E., 1969. "Comment on Solution of a Three-Dimensional Boundary Layer Flow with Separation," AIAA Journal, Vol. 7, No. 3.

14. Tracy, R.R., 1963. "Hypersonic Flow over a Yawed Circular Cone," Memo No. 69, Graduate Acro. Labs. Cal. Inst. of Tech.

15. Popinski, Z. "Three Dimensional Compressible Laminar Boundary Layers on Sharp and Blunt Circular Cones at Angle of Attack," University of Cincinnati, Aerospace Engineering Ph.D. dissertation; also to appear as a NASA Contractors Report.

16. Jones, D.J., "Tables of Inviscid Supersonic Flow about Circular Cones at Incidence $\gamma=1.4$," AGARDOGRAPH 137, Part I and II.

17. Rakich, J.V. and Cleary, J.W., 1970. "Theoretical and Experimental Study of Supersonic Steady Flow Around Inclined Bodies of Revolution," AIAA Journal, Vol. 8, No. 3.

18. Richtmyer, R.D., 1957. Difference Methods for Initial Value Problems, Interscience Publishers, Inc., New York.

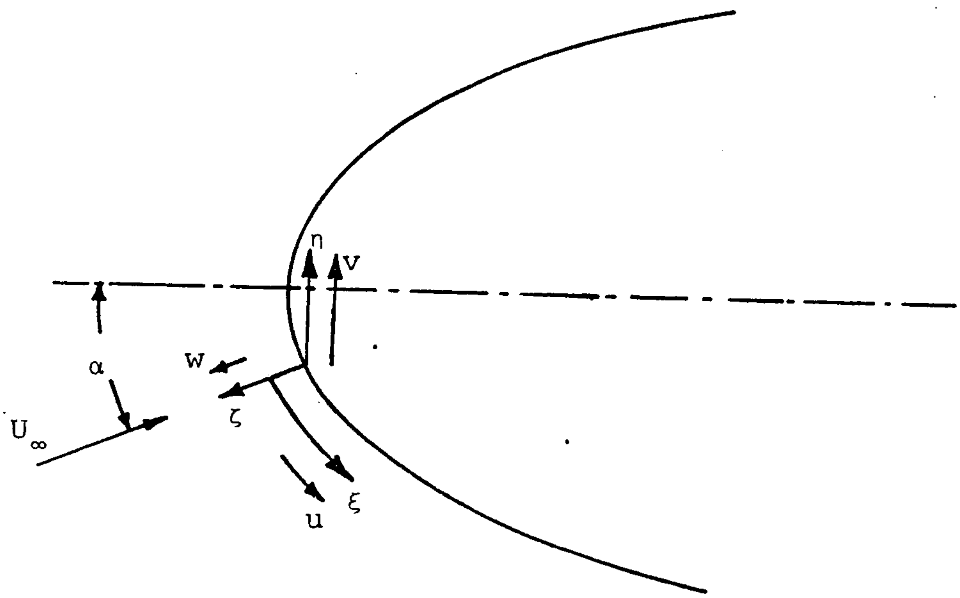

$$d\bar{S}_1 = \bar{h}_1 \, d\zeta$$

$$d\bar{S}_2 = \bar{h}_2 \, d\eta$$

$$d\bar{S}_3 = \bar{h}_3 \, d\zeta$$

Fig. 2.1. BODY ORIENTED CO-ORDINATE SYSTEM

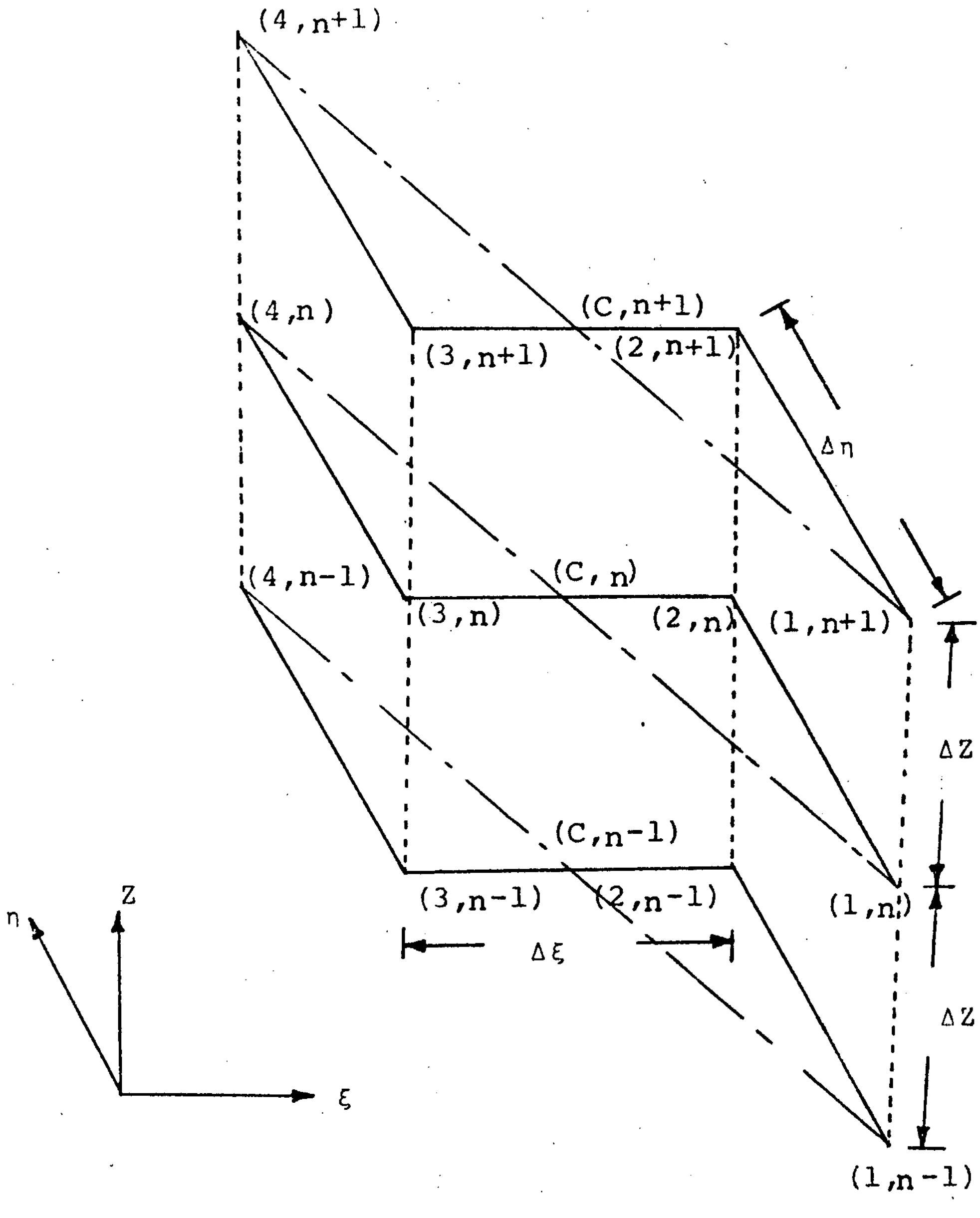

Fig. 3.1. FINITE DIFFERENCE SCHEME USED IN GENERAL CASE

E

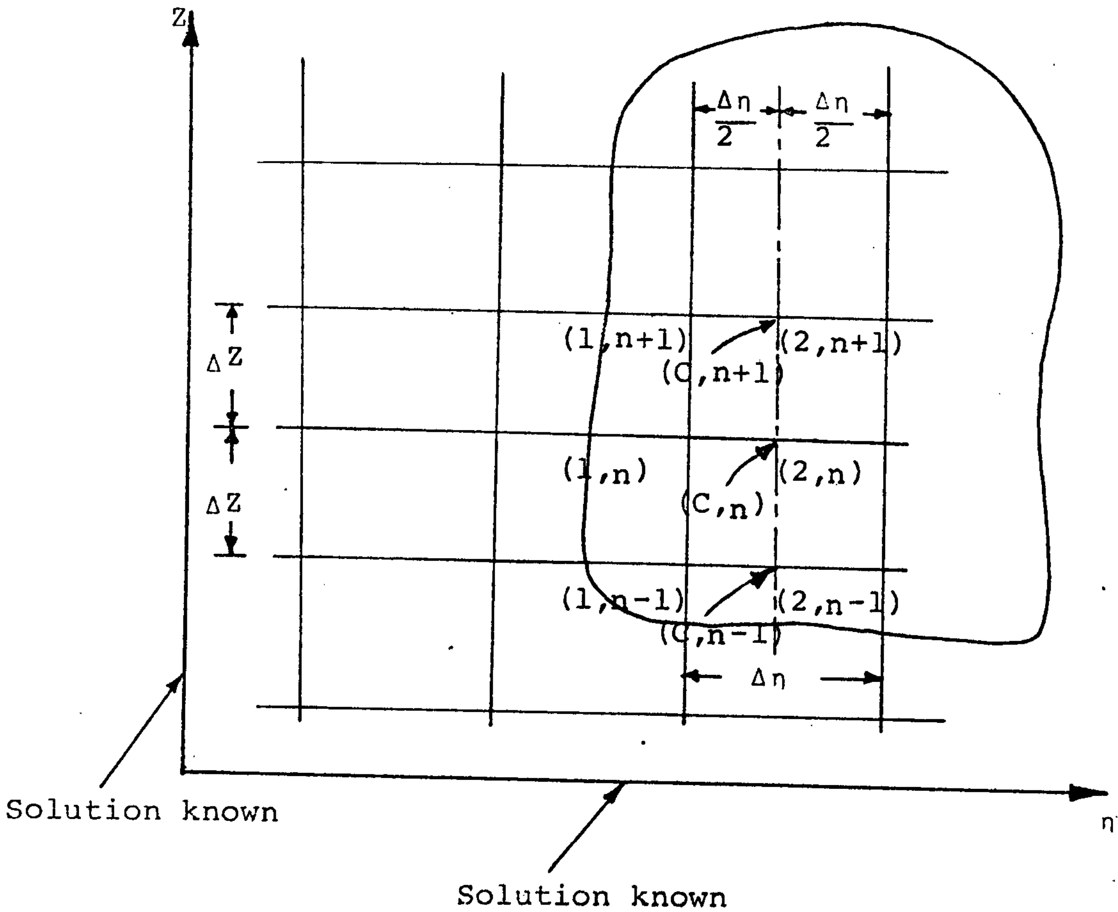

Fig. 3.2a. FINITE DIFFERENCE SCHEME USED WHEN SIMILARITY EXISTS IN ξ-DIRECTION

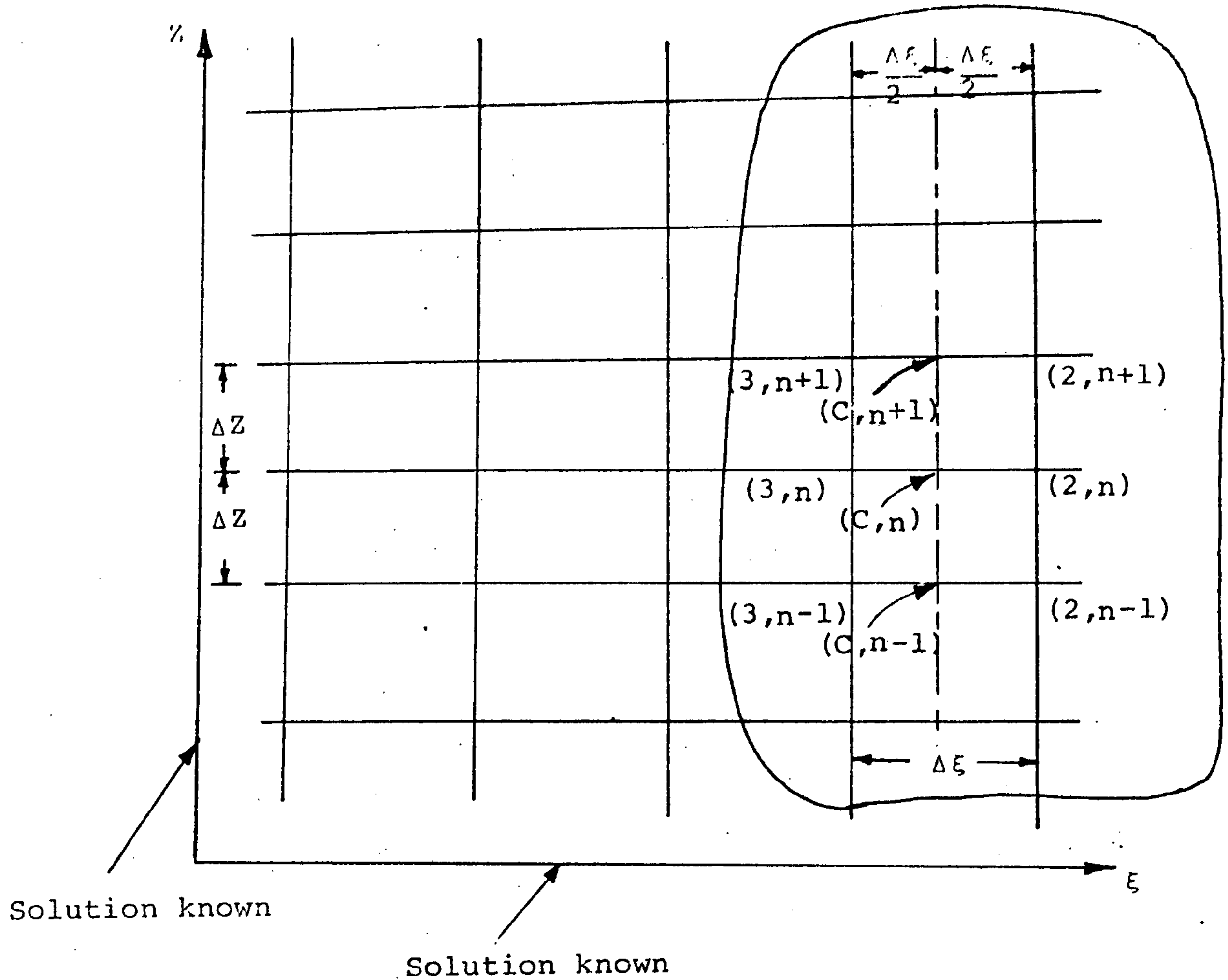

Fig. 3.2b. FINITE DIFFERENCE SCHEME USED WHEN SIMILARITY EXISTS IN η-DIRECTION

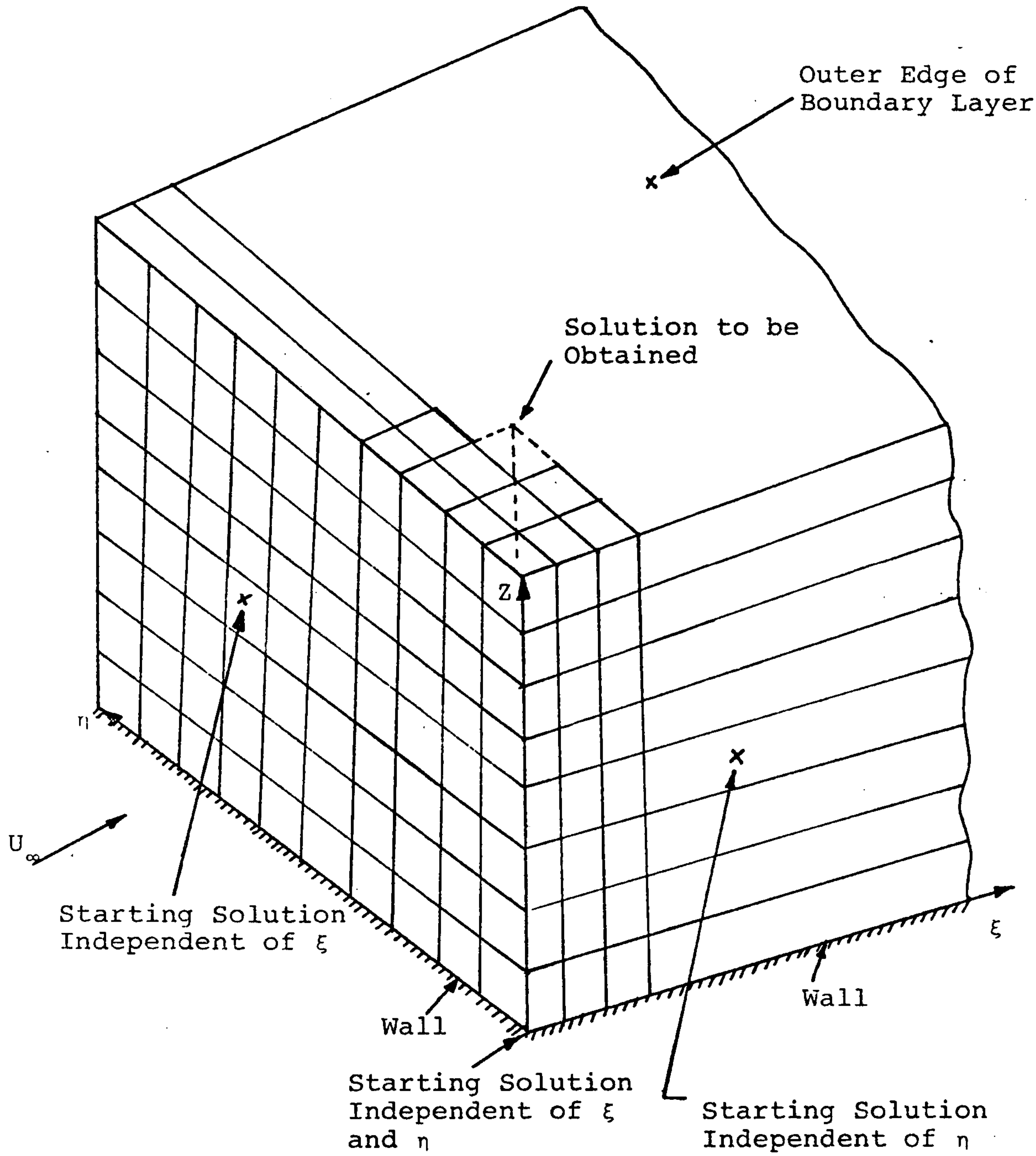

Fig. 3.3. GENERAL SET UP FOR STEP-BY-STEP INTEGRATION

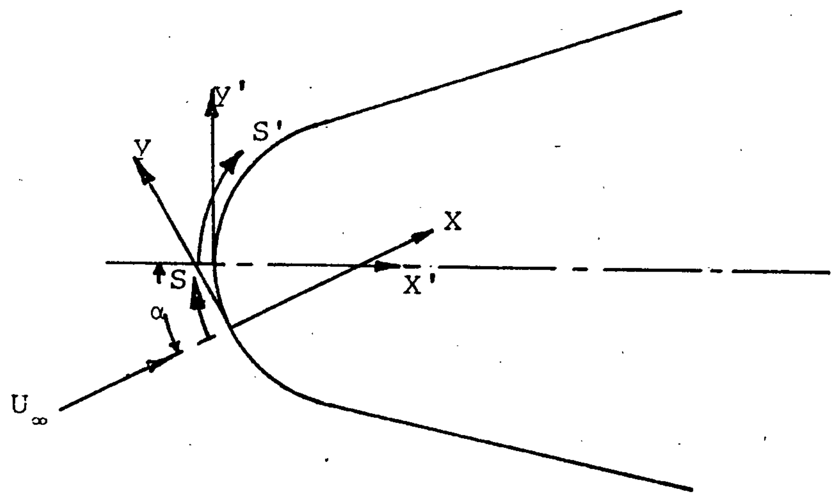

Fig. 4.1. CO-ORDINATE SYSTEM USED FOR SPECIFYING INVISCID DATA FOR SYMMETRIC SPHERE (x,y) AND FOR GENERAL 3-D BODY GEOMETRY (x',y')

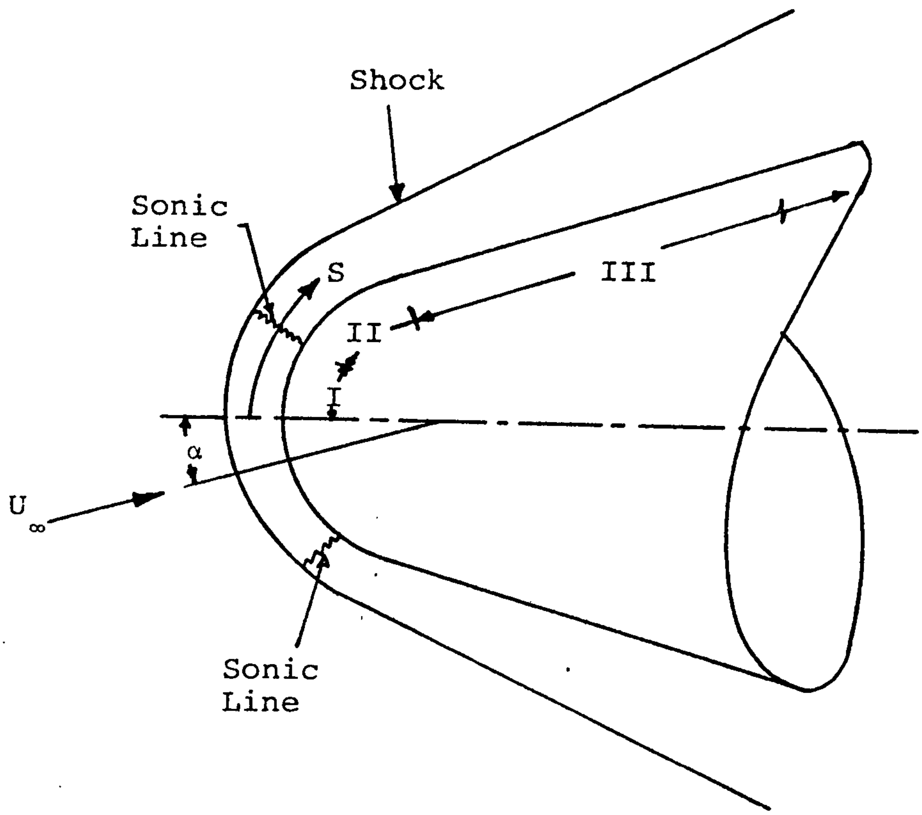

Fig. 4.2. SCHEMATIC DIAGRAM INDICATING THE THREE REGIONS WHERE SEPARATE POLYNOMIALS ARE USED FOR EACH REGION TO OBTAIN THE INVISCID PRESSURE DATA

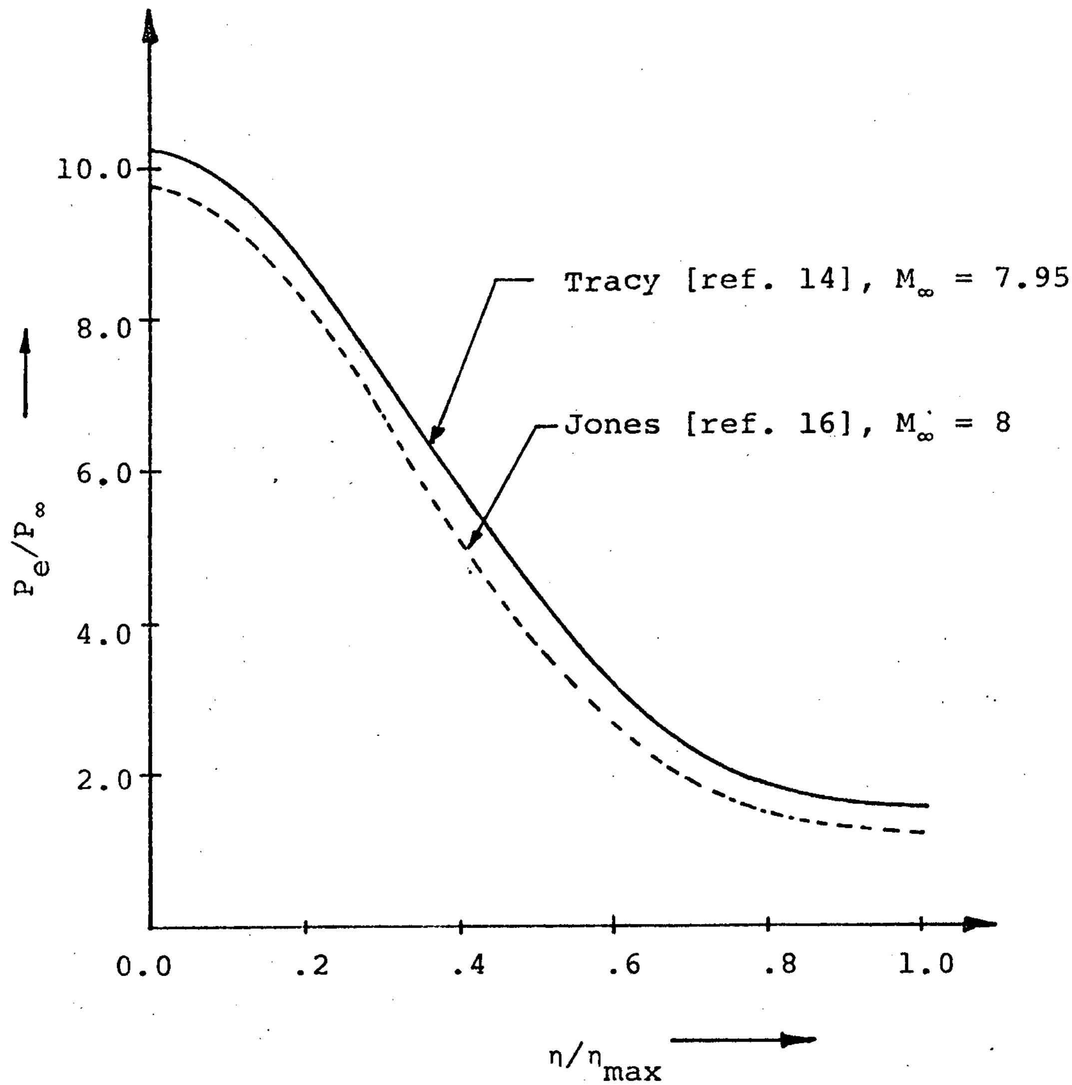

Fig. 5.1. PRESSURE DISTRIBUTION ON SHARP CIRCULAR CONE AT 8° ANGLE OF ATTACK

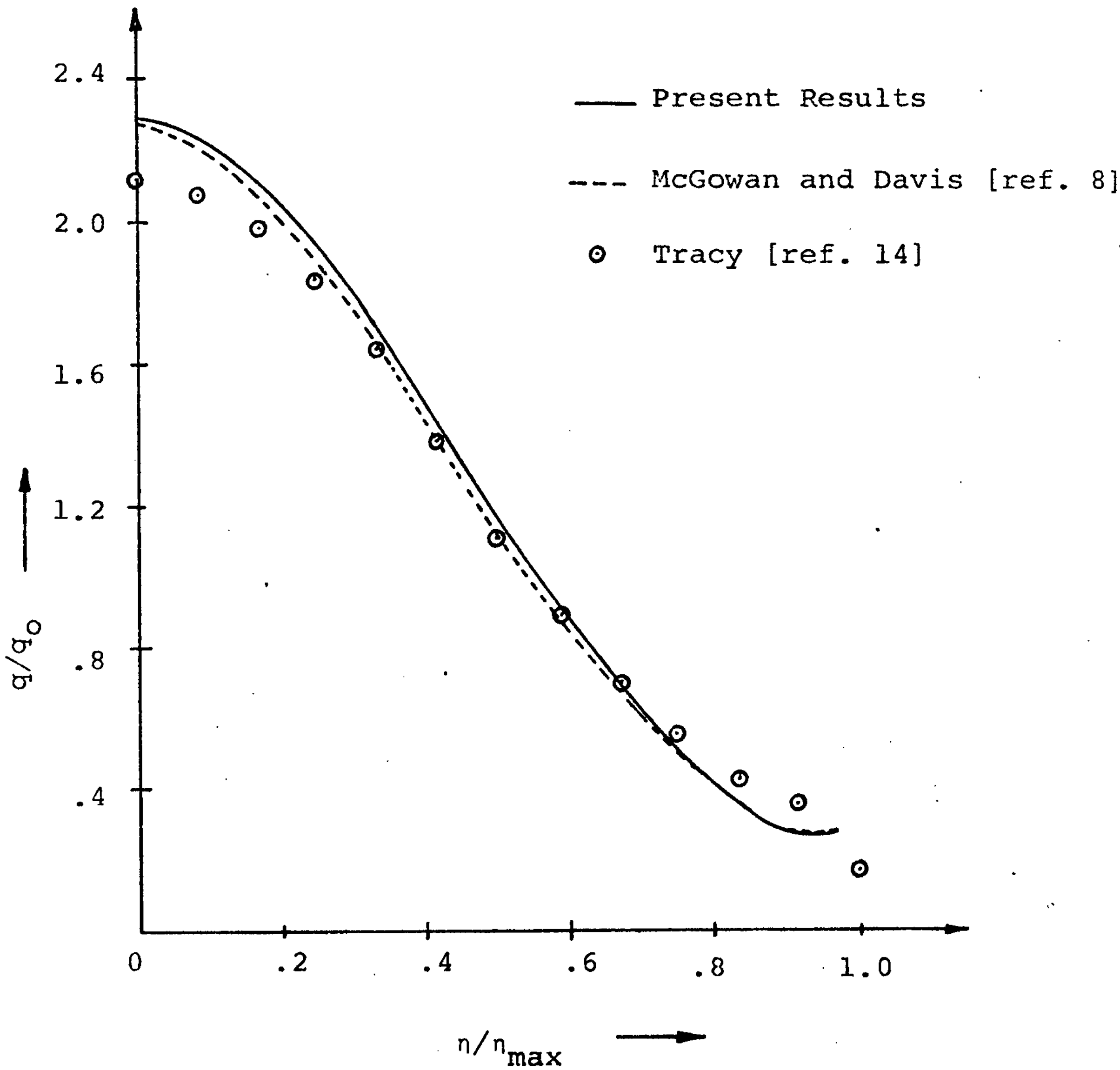

Fig. 5.2. HEAT TRANSFER RATE DISTRIBUTION
ON SHARP CIRCULAR CONE AT 8°
ANGLE OF ATTACK

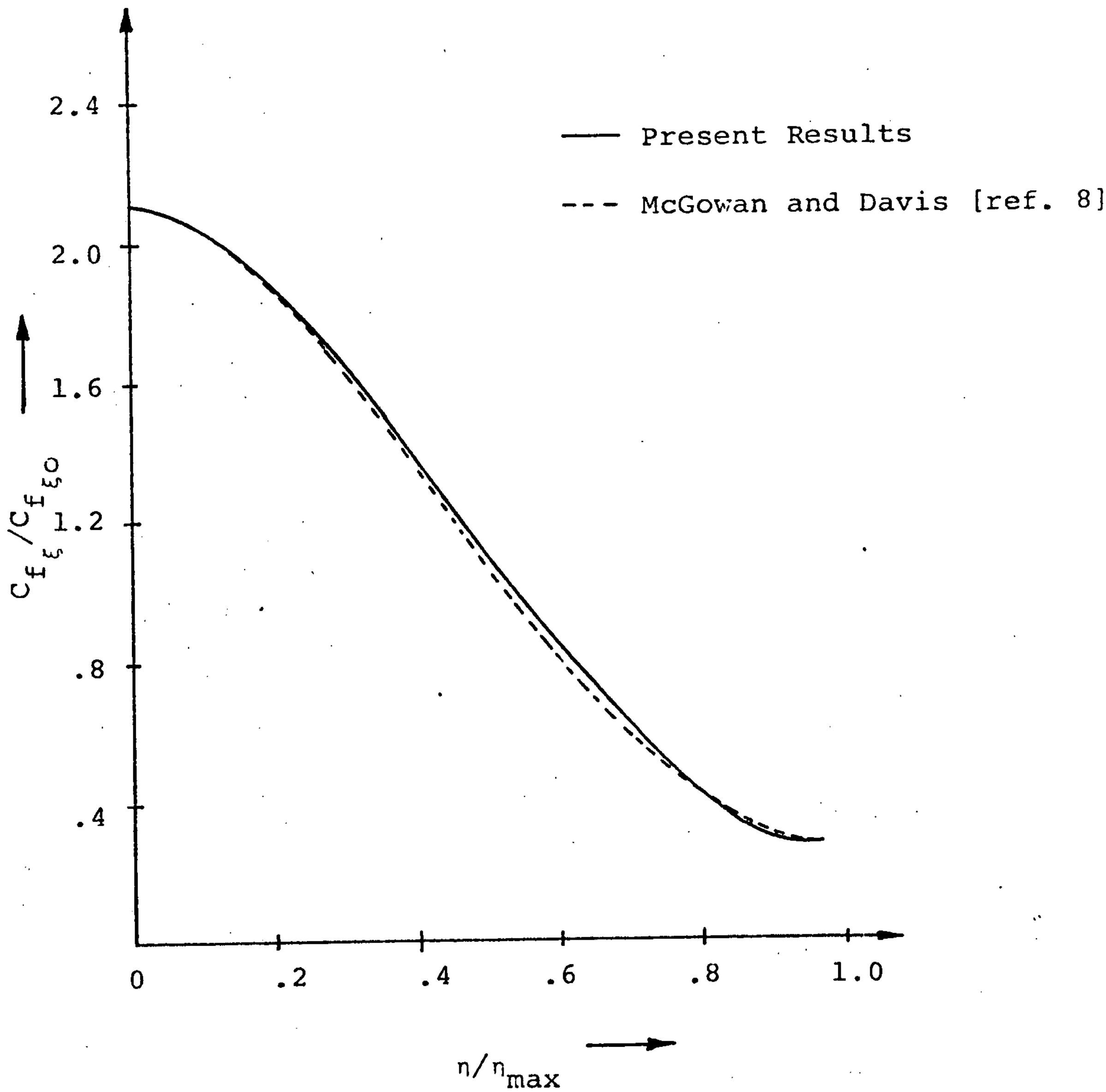

Fig. 5.3. LONGITUDINAL SKIN FRICTION DISTRIBUTION ON SHARP CIRCULAR CONE AT 8° ANGLE OF ATTACK

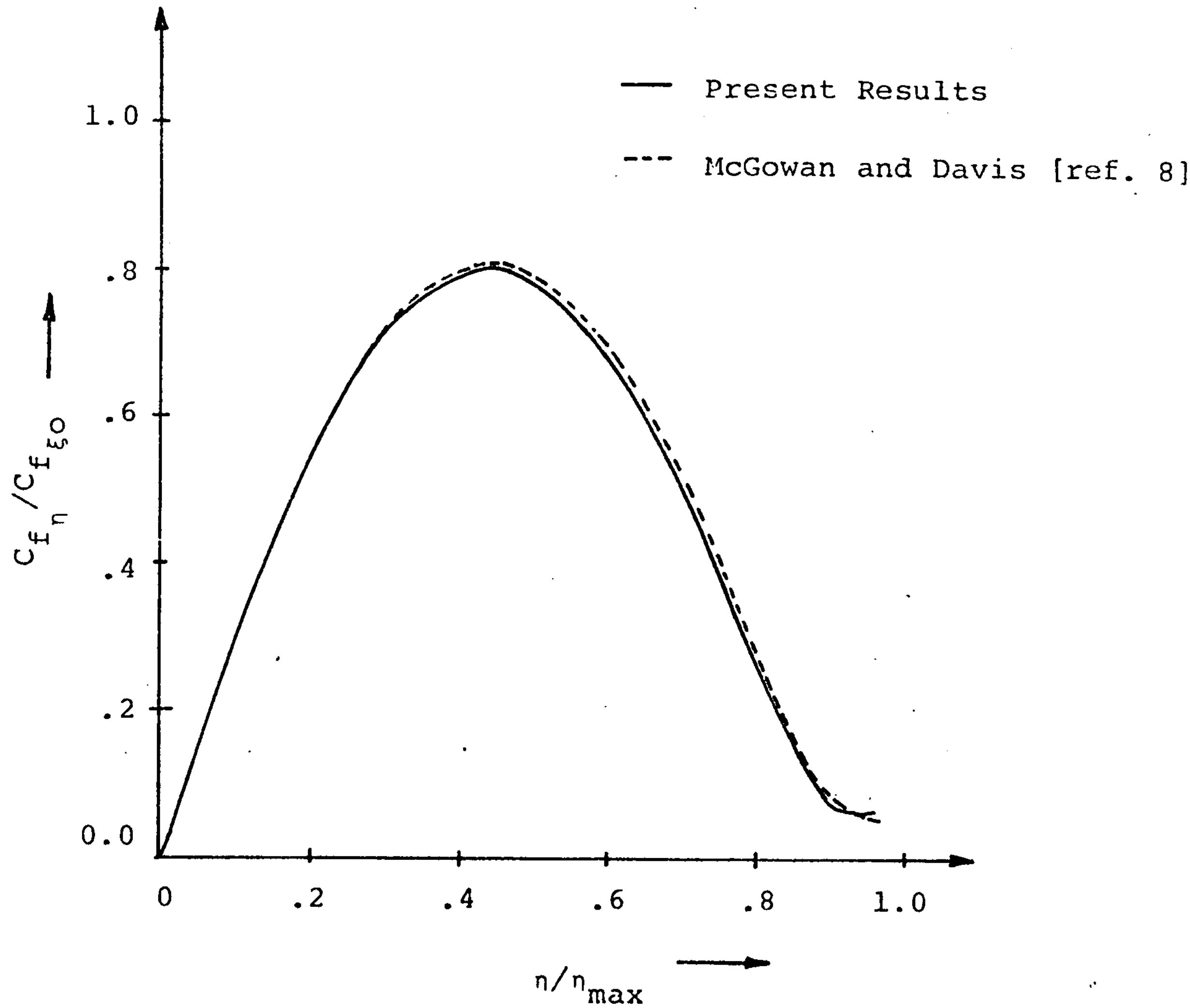

Fig. 5.4. TRANSVERSE SKIN FRICTION DISTRIBUTION ON SHARP CIRCULAR CONE AT 8° ANGLE OF ATTACK

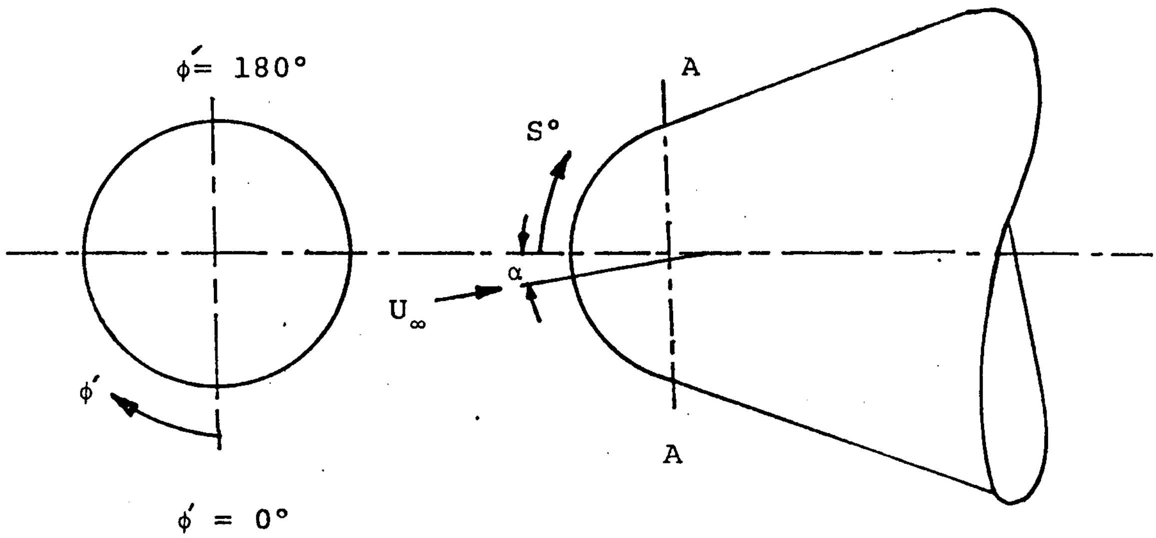

Fig. 5.5. SCHEMATIC DIAGRAM OF CO-ORDINATES USED TO PRESENT RESULTS FOR SPHERICALLY BLUNTED CONE AT AN ANGLE OF ATTACK

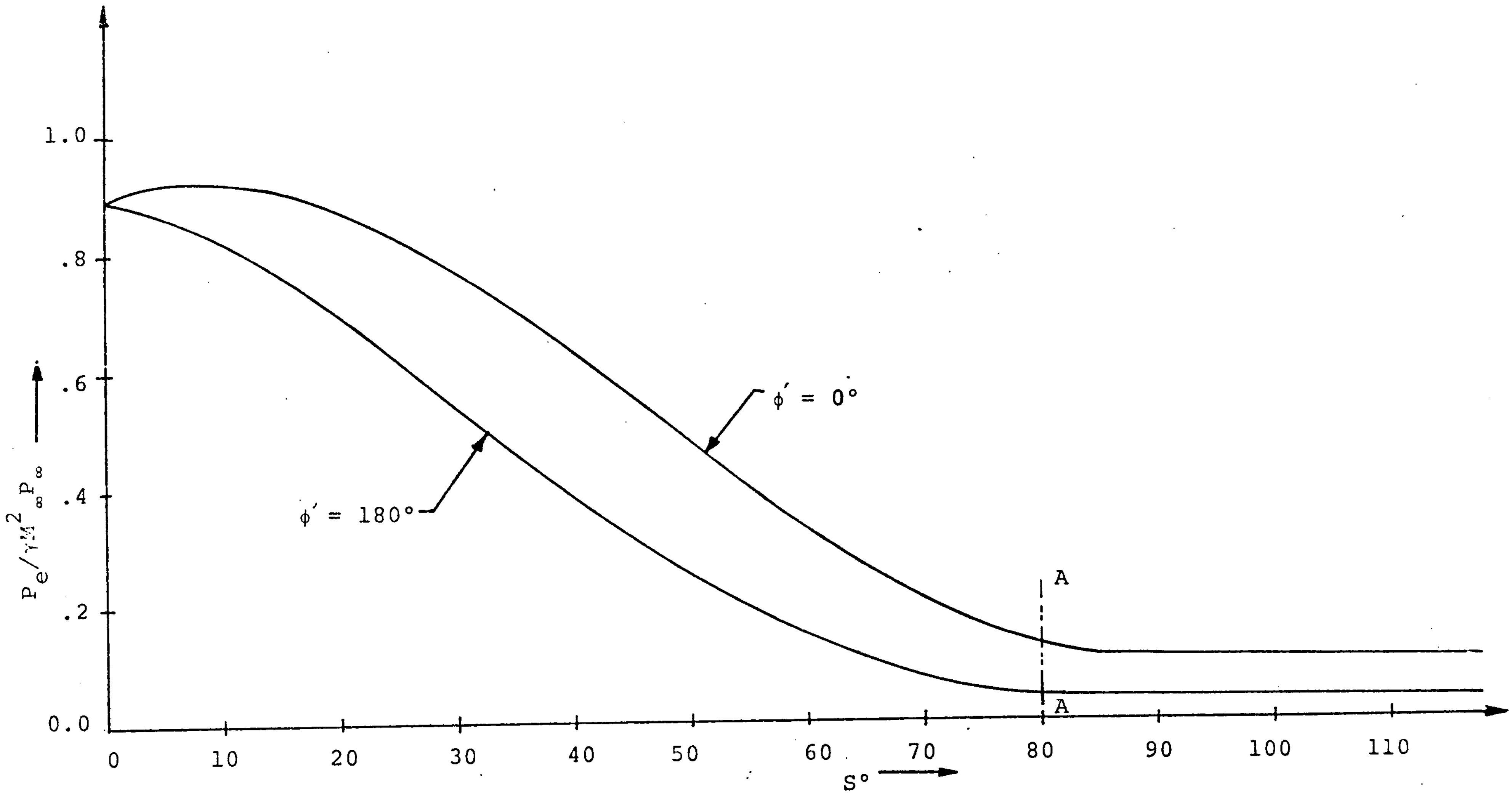

Fig. 5.6. PRESSURE DISTRIBUTION FOR BLUNTED CONE

AT 8° ANGLE OF ATTACK

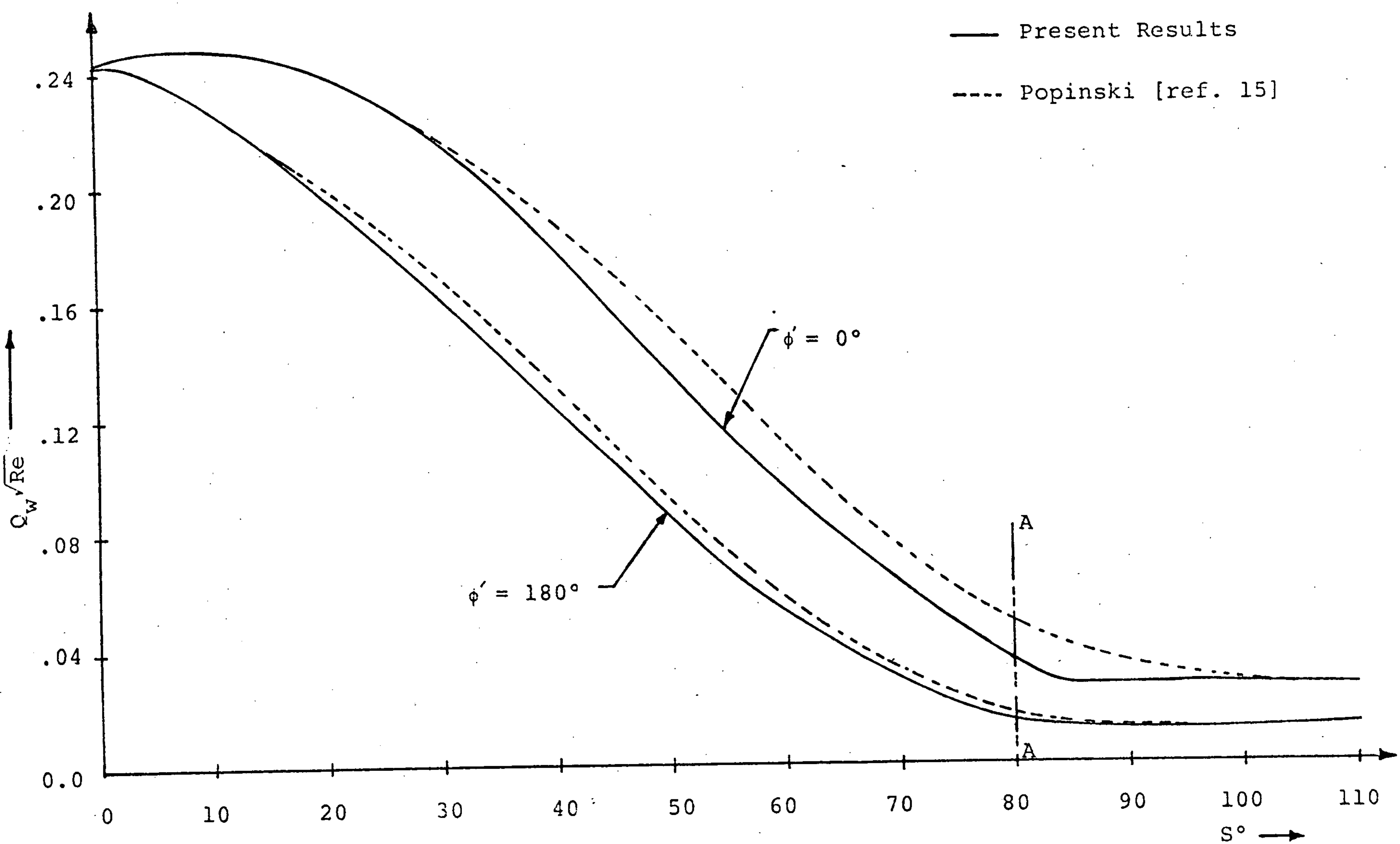

Fig. 5.7. HEAT TRANSFER RATE DISTRIBUTION FOR BLUNTED CONE AT 8° ANGLE OF ATTACK

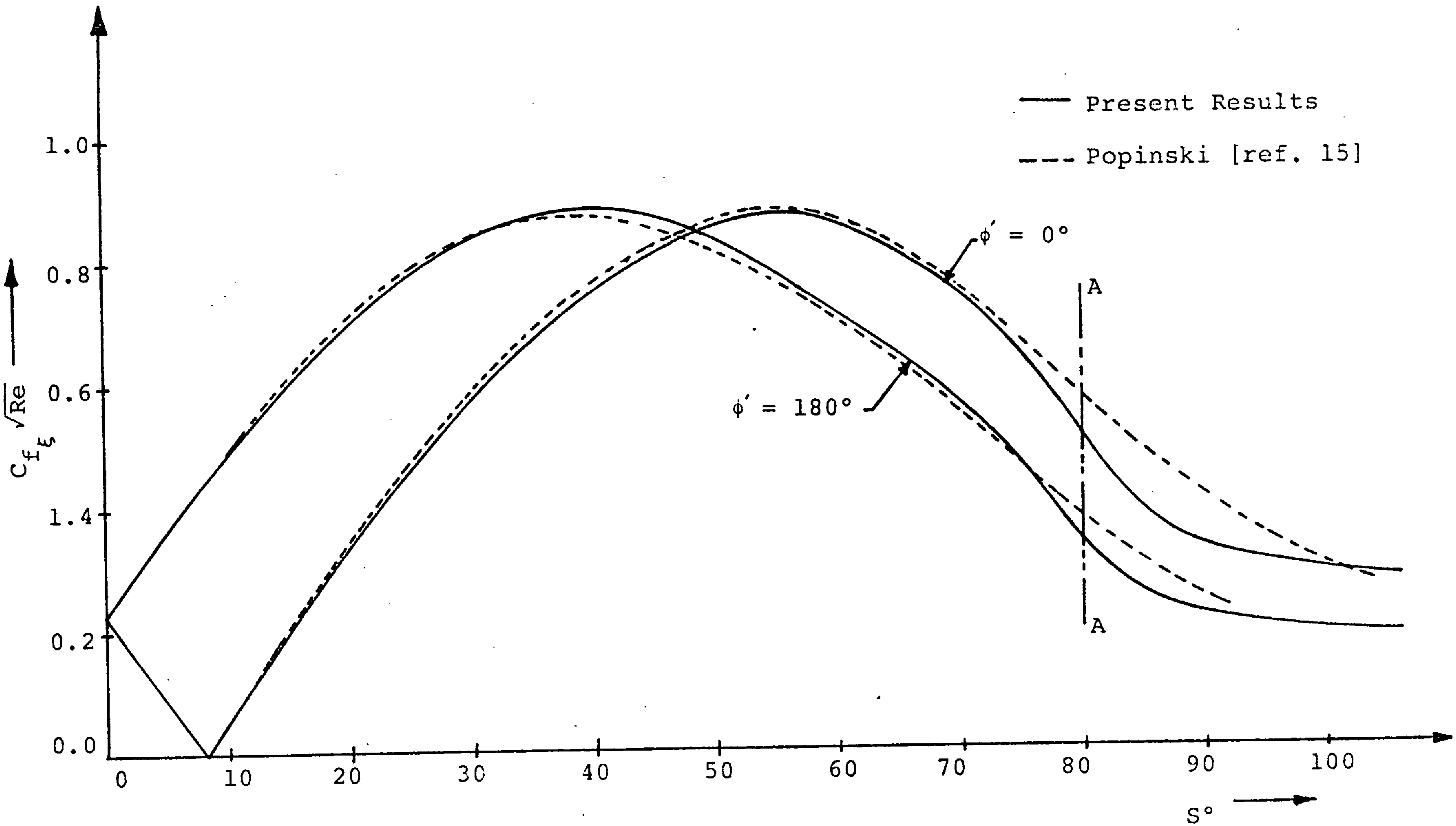

Fig. 5.8. LONGITUDINAL SKIN FRICTION DISTRIBUTION FOR BLUNTED CONE AT 8° ANGLE OF ATTACK

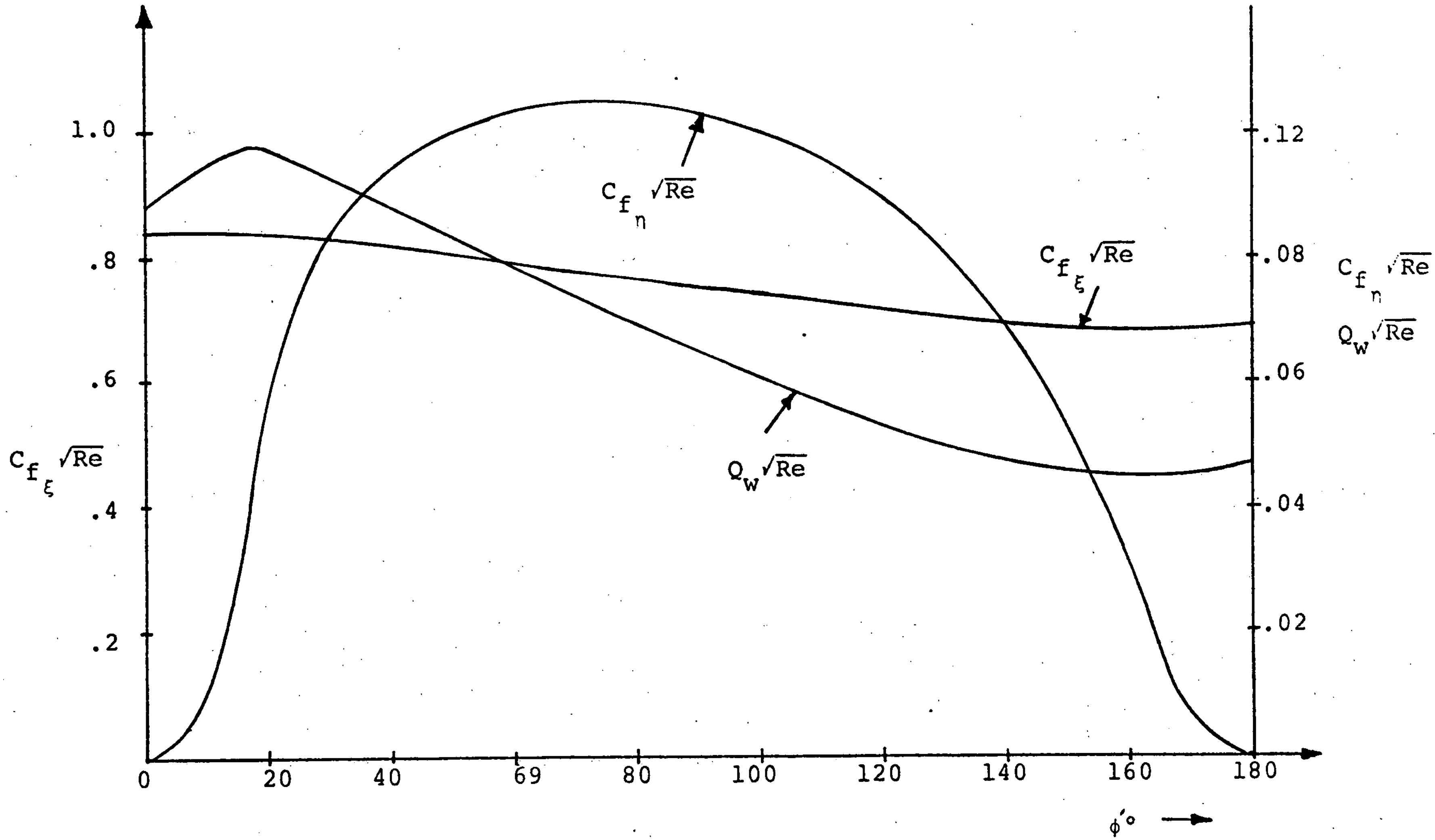

Fig. 5.9. VARIATION OF HEAT TRANSFER RATE, LONGITUDINAL AND TRANSVERSE SKIN FRICTION AROUND BLUNTED CONE AT 8° ANGLE OF ATTACK (S=62°)

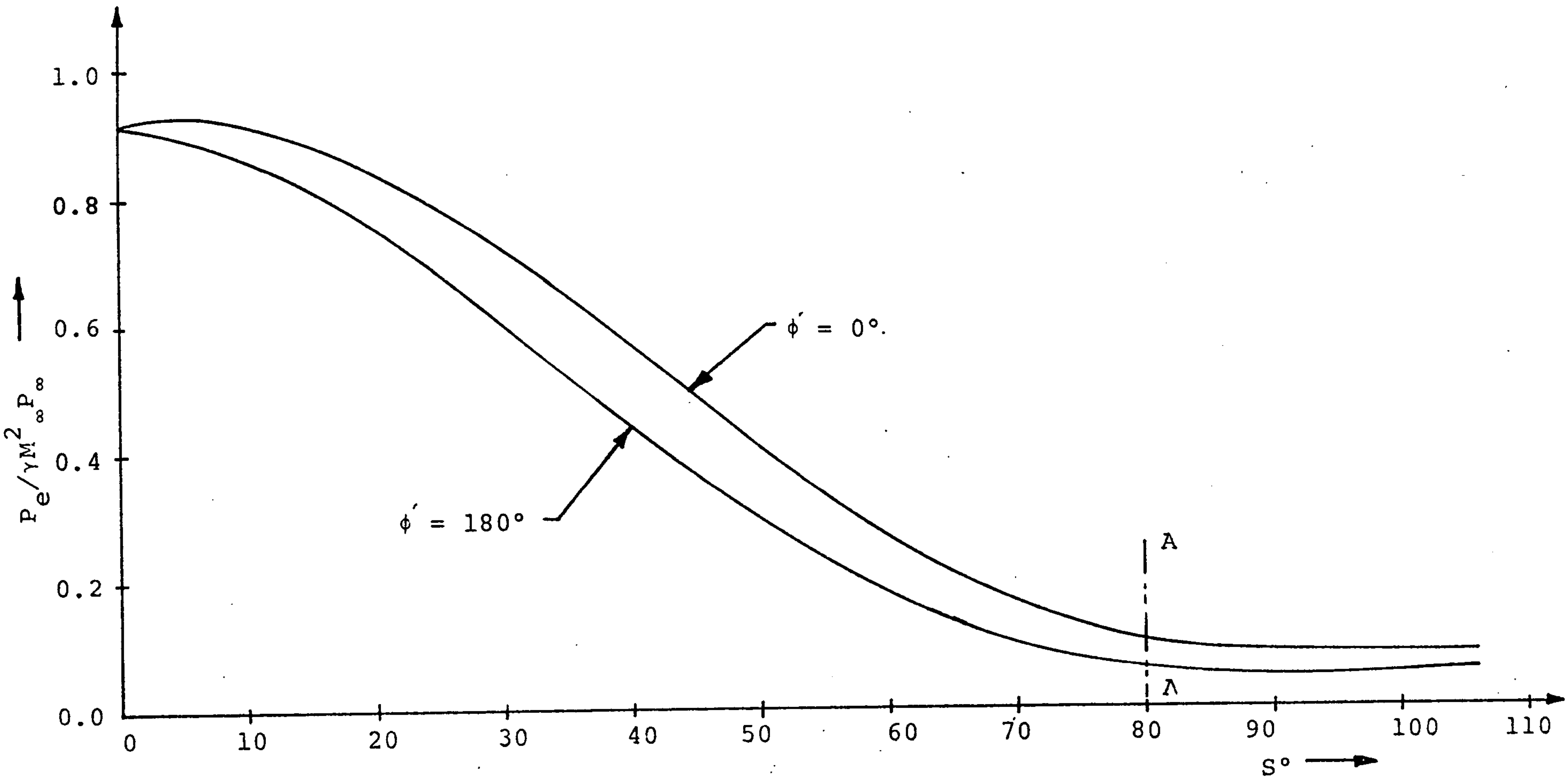

Fig. 5.10. PRESSURE DISTRIBUTION FOR BLUNTED CONE AT 4° ANGLE OF ATTACK

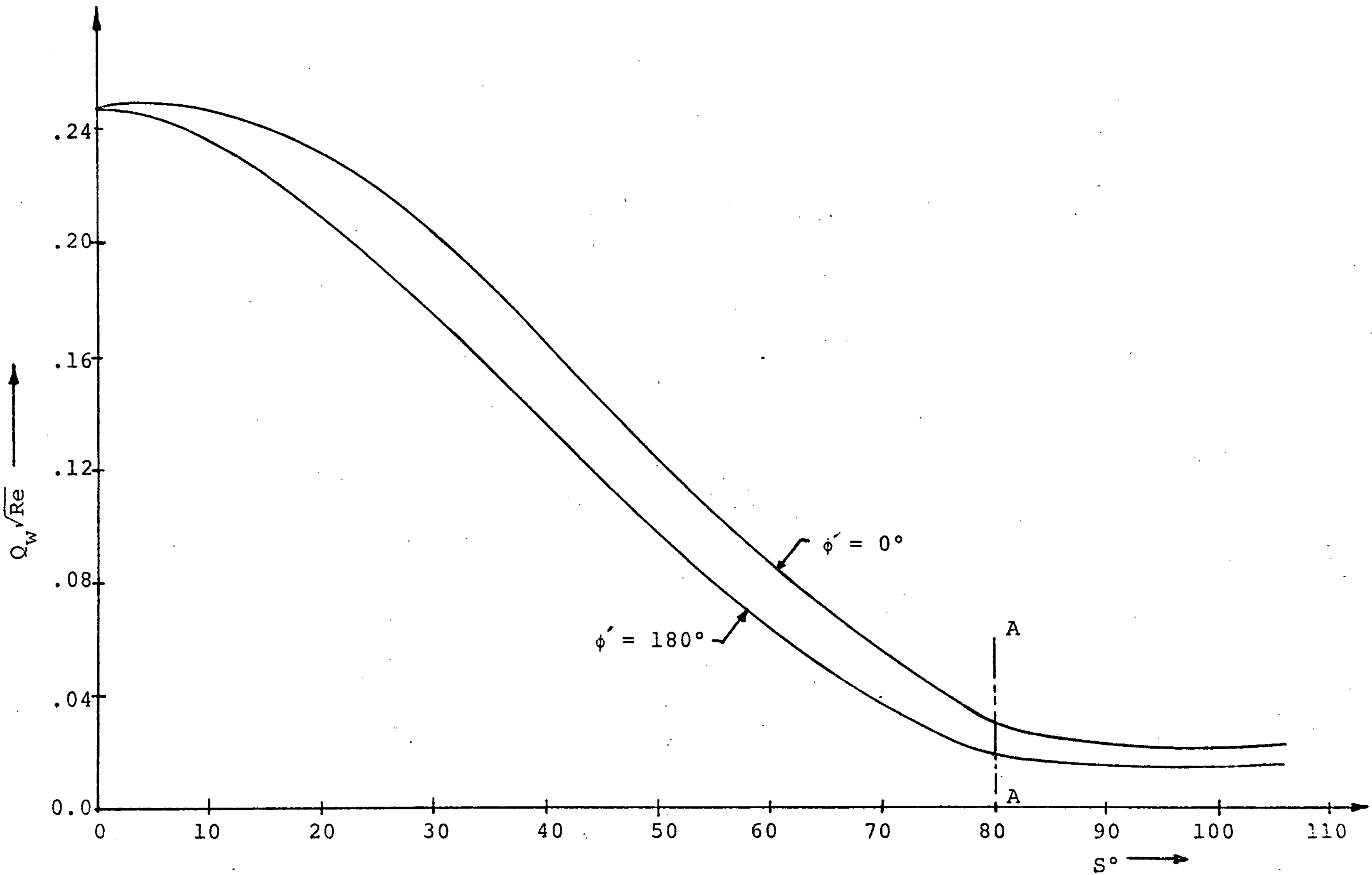

Fig. 5.11. HEAT TRANSFER RATE DISTRIBUTION FOR BLUNTED CONE AT 4° ANGLE OF ATTACK

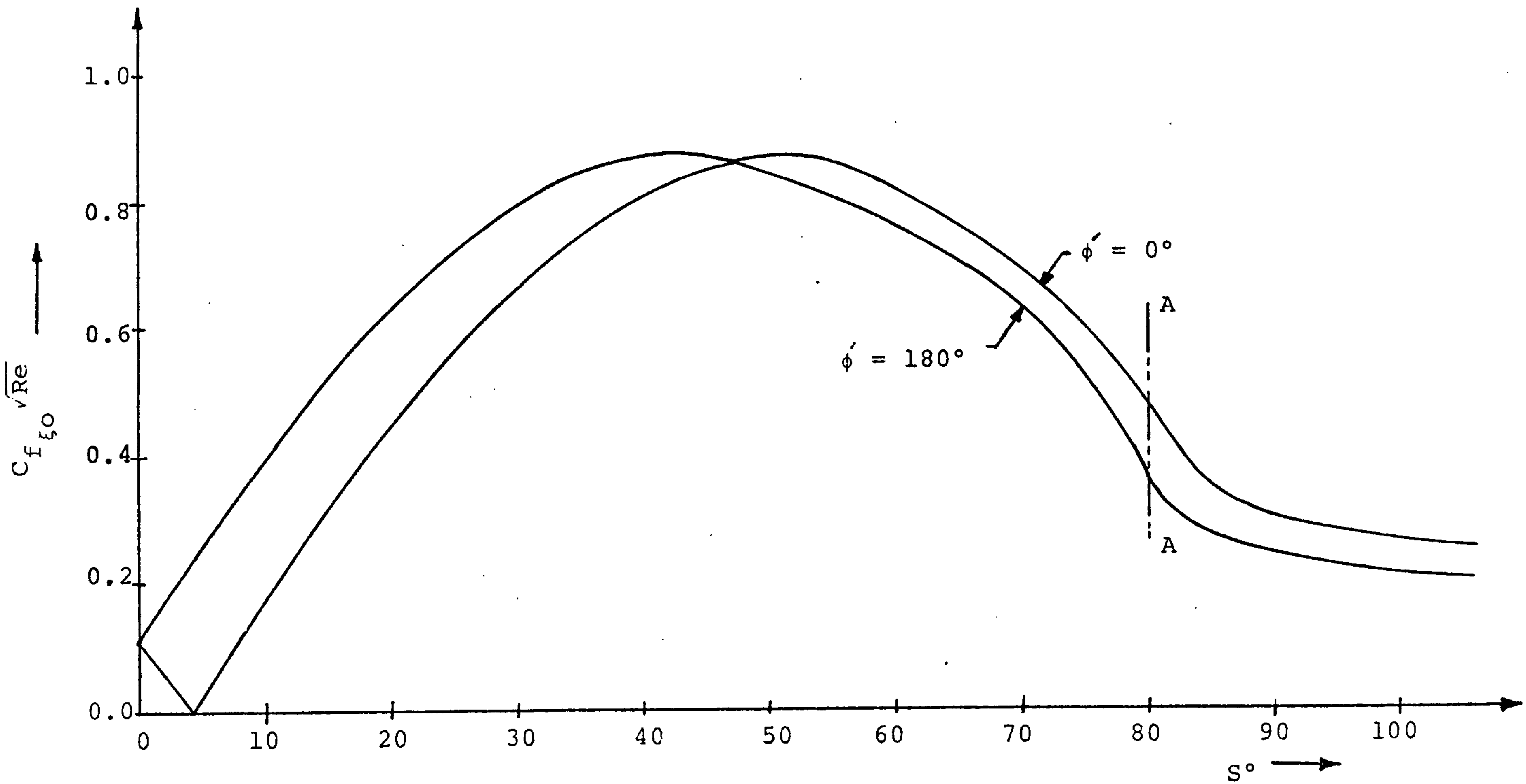

Fig. 5.12. LONGITUDINAL SKIN FRICTION DISTRIBUTION FOR BLUNTED CONE AT 4° ANGLE OF ATTACK

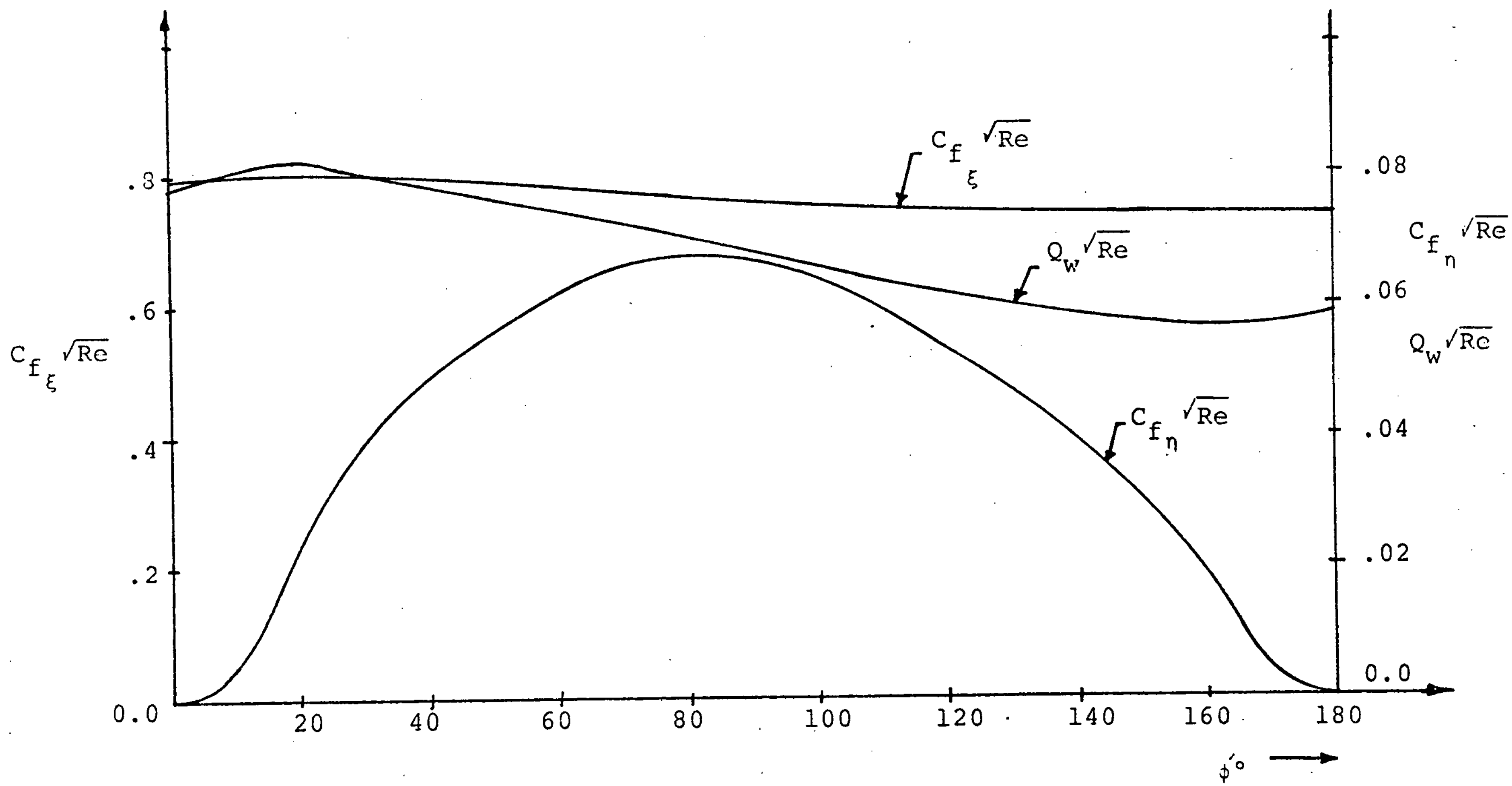

Fig. 5.13. VARIATION OF HEAT TRANSFER RATE, LONGITUDINAL AND TRANSVERSE SKIN FRICTION AROUND BLUNTED CONE AT 4° ANGLE OF ATTACK (S=62°)